REPUBLIC OF TÜRKİYE

ALTINBAŞ UNIVERSITY

Institute of Graduate Studies

Information Technologies

USING ARTIFICIAL INTELLGENCE TO IDENTFY SKIN CANCER

Ammar Maher Mohammed ALSARRAF

Master's Thesis

Supervisor

Prof. Dr. Osman Nuri UÇAN

Istanbul, 2023

USING ARTIFICIAL INTELLGENCE TO IDENTFY SKIN CANCER

Ammar Maher Mohammed ALSARRAF

Information Technologies

Master's Thesis

ALTINBAŞ UNIVERSITY

2023

The thesis titled USING ARTIFICIAL INTELLIGENCE TO IDENTIFY SKIN CANCER prepared by AMMAR MAHER MOHAMMED AL-SARRAFand submitted on 14/04/2023 has been **accepted unanimously** for the degree of Master of Science in Information Technologies.

_____

Prof. Dr. Osman Nuri UÇAN

Supervisor

Thesis Defense Committee Members:

Prof. Dr. Osman Nuri UÇAN	Department of Electrical and Electronic Engineering, Altınbaş University	_____
Asst. Prof. Dr. Sefer KURNAZ	Department of Computer Engineering, Altınbaş University	_____
Assoc. Prof. Dr. Adel Deniz DURU	Department of Sports and Health Sciences, Marmara Üniversitesi	_____

I hereby declare that this thesis meets all format and submission requirements of a Master's thesis.

Submission date of the thesis to Institute of Graduate Studies: ___/___/___

I hereby declare that all information/data presented in this graduation project has been obtained in full accordance with academic rules and ethical conduct. I also declare all unoriginal materials and conclusions have been cited in the text and all references mentioned in the Reference List have been cited in the text, and vice versa as required by the abovementioned rules and conduct.

Ammar Maher Mohammed ALSARRAF

Signature

DEDICATION

I dedicate this thesis to my family, who have always supported and believed in me. Without their love and encouragement, I would not have been able to complete this work.

I would also like to thank my supervisor, who provided me with guidance and support throughout the process.

Finally, I thank my friends and colleagues, who provided me with valuable insights and feedback during the writing process.

Thank you all for helping me to achieve this milestone.

PREFACE

This thesis is focused on the detection and classification of melanomas using teledermatology. Tele dermatology is the use of medical technology to diagnose and treat skin, nails and hair diseases. The goal of this thesis is to explore the potential for tele dermatology to detect and classify melanomas through the analysis of skin lesions.

The research presented in this thesis is based on the data collected from a study of tele dermatology images of skin lesions from patients who were suspected of having melanoma. The data was generated from a variety of sources, including clinical images, pathology slides, and data from a large database of tele dermatology images. By analysing the data, we have developed a method for detecting and classifying melanomas using tele dermatology.

This thesis will provide an overview of the current state of tele dermatology and its potential to detect and classify melanomas. We will also discuss the methods used in the study, and the results that were obtained. In addition, we will discuss the implications of our findings and the potential applications of tele dermatology for the early detection and classification of melanomas.

Finally, this thesis will provide some recommendations for improving tele dermatology technology in order to increase its accuracy.

.

ABSTRACT

USING ARTIFICIAL INTELLGENCE TO IDENTFY SKIN

ALSARRAF, Ammar Maher Mohammed

M.Sc., Information Technologies Department, Altınbaş University,

Supervisor: Prof. Dr. Osman Nuri UCAN

Date: April / 2023

Pages: 69

Melanoma is among the most severe types of skin cancer. By segmenting lesions, carrying out fundamental processing, extracting dermo scope characteristics, and detecting diseases, image analysis algorithms can be used to autonomously diagnosis melanoma from dermo copy pictures. The improved early melanoma detection technique that is being suggested seeks to decrease both needless biopsies and mortality. We use the K-Means clustering method, thresholding for lesion segmentation, Sobel operator, median filter, GLCM and LBP features for feature extraction, and the Support Vector Machine (SVM) classification to categorize the ISIC archive dataset. 93.28% accuracy was obtained with the findings. Additionally, clinical pictures can be sent to a dermatologist remotely for review later using a networking app (like WhatsApp), enabling patient follow-ups during pandemics or for those residing in distant areas.

Keywords: GLCM, K-Means, Sobel, LBP, Support Vector Machine, WhatsApp.

TABLE OF CONTENTS

Pages

LIST OF TABLES

Pages

LIST OF FIGURES

Pages

ABBREVIATIONS

AC	:	Accuracy
AI	:	Artificial Intelligent
ANN	:	Artificial Neural Network
CCTV	:	Closed-Circuit television
COCO	:	Common Object on Context
CNN	:	Convolutional Neural Network
DCNN	:	Deep Convolutional Neural Network
DL	:	Deep Learning
GAN	:	General Advanced Networks
GPU	:	Graphic Processing Unit
GUI	:	Graphic User Interface
HOG	:	Histogram of Oriented Gradients
IOU	:	Intersection Over Union
LBP	:	Local Binary Pattern
ML	:	Machine Learning
$PREC$	:	Precision
RNN	:	Recurrent Neural Network
ROI	:	Region of Interest
SE	:	Sensitivity
ISIC	:	Skin Imaging Collaboration
SP	:	specificity
SGD	:	Stochastic Gradient Descent
SVM	:	Support Vector Machines
TD	:	Teledermatology
TP	:	True Positive
UAV	:	Unmanned Aerial Vehicle
YOLO	:	You Only Look Once

1. INTRODUCTION

Cutaneous malignancies are the most prevalent and least serious of all human malignancies, and the epidermis is thought to be the biggest tissue in the body. High rates of mortality and morbidity are associated with cutaneous malignancy, which is the most frequent kind of cancer globally [1], [2]. As the population ages and more people sustain UV damage to their skin, the incidence rate rises[3]. The death rate is very variable among the different types of skin cancer and among the subtypes within this classification[1]. Differentiating skin malignancies from benign lesions is an advanced skill that is rarely taught to medical professionals outside of dermatology[4].

Even though there is mounting evidence that training in this area improves medical students' and GPs' capacity to diagnose skin lesions, dermatologists and other medical professionals still get a disproportionately little amount of instruction in the field[4]. This can complicate the process of identifying and treating skin malignancies. [2]

1.1 MELANOMA

Melanoma is a type of cancer that begins in the skin and is caused by pigment-producing cells (melanocytes) in the epidermis. It is estimated that 57,043 people died from skin melanoma in 2020, making it the 13th most common cancer. There are four primary subtypes of cutaneous melanoma, and more than 30 rarer variants. In Sweden, there are around 7,000 new cases of melanoma or situ-melanoma diagnosed each year with a reported survival rate of 85%[5]. Teledermoscopy is a method of early detection which allows a family doctor to take pictures of a lesion and save them online for a dermatologist to examine. A machine learning system that can help the dermatologist find relevant structures in the lesion would be a great asset to this service. The first step of the procedure is for the dermatologist to examine the lesion for pattern and/or colour irregularities, and search for Clues, which are a set of potentially relevant characteristics. In cases where Clues and Chaos are present, it is often necessary to surgically remove the lesion for treatment[2].

1.2 TELEDERMATOLOGY (TD)

COVID-19 has led to the extensive use of Tele-dermatology (TD), which is a form of remote dermatology, to improve access to dermatology care. TD can be done through synchronous and asynchronous approaches, or a combination of both. Store-and-forward TD is useful in

underprivileged areas, but the need for a digital camera and computer can be a barrier to access for some regions. Teledermatology offers improved access to skin-related healthcare in rural areas, as well as decision support for general practitioners[6], [7].

1.3 RELATED WORKS

The three challenges for the ISBI 2018 challenge were lesion segmentation, dermoscopic feature extraction, and lesion classification, for which the International Skin Imaging Collaboration was responsible (ISIC), according to Codella N. et al. [8]. An expert used a binary mask to manually draw the lesion borders on 90 distinct images from the training dataset. Roughly 30% of the sample was cancerous. (273 images in the training set). Area Under Curve (AUC) and Average Precision were used in the categorization process, while pixel-level precision, specificity, the Dice coefficient, and the Jaccard index were used in the segmentation process. (AP).

Zhao Z. et al. [9] Fuzzy C-means and K-means are two recommended techniques for segmenting-colored images. Yunus K. et al. [10] showed how to use the Jaccard Index or Dice's Coefficient with the c-means and k-means clustering techniques for image segmentation and classification.

Nasir M. et al. [11] Two essential components for lesion analysis were proposed: a real-time sunburn warning and an automatic image analysis tool that incorporates image capture, hair removal and recognition, lesion segmentation, feature extraction, and classification. The proposed approach makes use of Pedro Hispano Hospital's dermo copy image collection (PH2), which contains nearly 200 ceroscopy images of benign, unusual, and malignant lesions. Normal, atypical, and melanoma images were accurately classified in 96.3%, 95.7%, and 97.5% of cases, respectively, in experiments.. [12].

Simin A. et al. [13] GLCM texture-based second-order statistical features for ANN-based skin cancer categorization have been suggested. Mohammed S. et al. [14] demonstrated how to detect skin conditions using texture-predicted characteristics from the GLCM. Several studies combined texture-predicted characteristics and other traits to increase categorization accuracy, focusing on contrast, correlation, energy, entropy, and homogeneity. Medical image analysis frequently employs texture-predicted features for medical detection, and achieves over 90% average accuracy using neural networks and SVM as predictors. [15].

Muhammad Ali Farooq et al. based on probabilistic methods, an improved ALDS framework was created [16], using active contours and a watershed combined mask for mole

segmentation and SVM and a neural classifier for mole categorization. The remaining characteristics decide whether the tumor is melanoma after lesion segmentation.

Senan E. et al. [17] proposed combining the finest features of MRELBP and DRLBP to create a feature extraction technique for skin cancer lesions. (Median Robust Extended Local Binary Pattern). Based on characteristics taken from the pictures, an SVM classifier classifies them.

Prathiba M. et al. [18] suggested using deep learning methods for precise lesion location and melanoma detection. Convolutional neural networks (CNN) are frequently used for melanoma identification because they closely resemble the human visual brain.

1.4 PROBLEM STATEMENT

Recently, deep learning has been used in the field of teledermatology to diagnose skin cancer at off-site locations. This study aims to develop a deep learning system that can identify skin lesions in images as skin cancer.. The model should be able to be used in a variety of teledermatology settings and should be durable, precise, and dependable. The model should also be able to differentiate between various forms of skin cancer, including melanoma, basal cell carcinoma, and squamous cell carcinoma. Additionally, the model should be able to differentiate between normal and malignant tumors. Finally, the model should be able to provide the user with a confidence score for the diagnosis.

Skin cancer may be identified and diagnosed using deep learning. Convolutional neural networks (CNNs) are used to examine pictures of skin lesions, a doctor can diagnose the presence of melanoma and other types of skin cancer. CNNs can be trained to recognize features in an image that indicate the presence of cancer, such as color, texture, and shape. CNNs can also be used to predict the probability of a skin lesion being cancerous, as well as to classify the type of cancer present. By combining deep learning with other methods, such as medical imaging, pathology, and genetic testing, a doctor can have a more comprehensive understanding of a patient's skin cancer diagnosis.

1.5 AIM OF THESIS

The purpose of this thesis is to locate and develop a suitable machine learning model for detecting Chaos in dermatoscopic image data. This necessitates that the model detects colour and pattern differences between skin lesions.

1.6 THE CONTRIBUTIONS OF THESIS

The proposed system's key features can be summarized as follows:

i. i. To handle over-fitted training data, the SVM classifier is used to quickly and accurately develop a melanoma classification model.

ii. ISIC-2016's standard database and real patient images with a variety of distortions, including blurring, chrominance and intensity variations, the presence of hair and small blood vessels, and high-density noise, are used to train and test this model.

iii. Reducing the risk of COVID-19 spread, improving the classification of melanoma in underserved regions, and diagnosing common ambulatory dermatoses remotely all using the TD method (via WhatsApp).

1.7 THE LAYOUT OF THESIS

The remaining parts of the thesis, after chapter one, will be organized as follows:

a. The theoretical underpinnings of mood recognition techniques, as well as the datasets utilized in this subject, are demonstrated in Chapter Two.

b. The planned facial recognition system is described in Chapter Three, along with detailed methods and block schematics depicting the system's main components.

c. In Chapter Four, We'll demonstrate how the suggested approach was used and go through the project's results.

d. • The conclusions and suggestions for more study are offered in Chapter Five.

2. THEORETICAL BACKGROUND

Deep learning is a type of artificial intelligence (AI) that is used to increase the precision of a skin cancer diagnosis. Artificial neural networks are used in deep learning to categorize skin lesions from a vast collection of photos into several subtypes of skin cancer [19].

The goal of deep learning for skin cancer is to make a computer-aided diagnostic system (CAD) that can accurately diagnose skin cancer in real-time. This would make skin cancer diagnosis more accessible and reduce the burden of a manual diagnosis[20].

A convolutional neural network (CNN) is trained to properly categorize photos of skin lesions into several categories of skin cancer by using a vast collection of photographs of skin lesions. By giving it photos of skin lesions and having it categorize them based on their kind, the CNN is taught. As a result, the network may learn to distinguish various skin cancer kinds [21].

Once the network is trained, it can be used to accurately classify new images of skin lesions and diagnose skin cancer with greater accuracy than manual diagnosis. This could help reduce the burden of manual diagnosis and make skin cancer diagnosis more accessible.

2.1 SKIN CANCER DETECTION TECHNIQUES

The field of skin cancer diagnosis has seen an increase in the use of deep learning algorithms. These methods have been utilized to create automated systems that can recognize and categorize skin lesions, assisting doctors in making an accurate and speedy skin cancer diagnosis, This section explains the most important methods for skin detection used, as shown in figure (2.1 a-d):

2.1.1. Image Segmentation

Image segmentation is a powerful technique used to accurately identify and localize suspicious skin lesions for skin cancer detection. It involves the division of an image into regions of interest and is accomplished through a combination of convolutional neural networks (CNNs) and other deep learning techniques.

2.1.2. Transfer Learning

Transfer learning is a process by which a pre-trained model can be used to solve a new problem. This technique has been used to develop deep learning models for skin cancer detection. In this approach, a neural network is trained on a large dataset of images of different skin lesions and then used to identify and classify skin lesions in new images.

2.1.3. Generative Adversarial Networks (GANs)

Realistic pictures of skin tumors have been produced using neural networks called generative adversarial networks (GANs). A deep learning algorithm can then be trained using these pictures to precisely detect and categorize skin lesions.

2.1.4. Recurrent Neural Networks (RNNs)

Recurrent neural networks (RNNs) are a particular kind of neural network that have been applied to the analysis of sequence data, including photographs. RNNs may be used to evaluate photos of skin lesions over time and find changes that can point to the existence of skin cancer in the context of skin cancer detection.

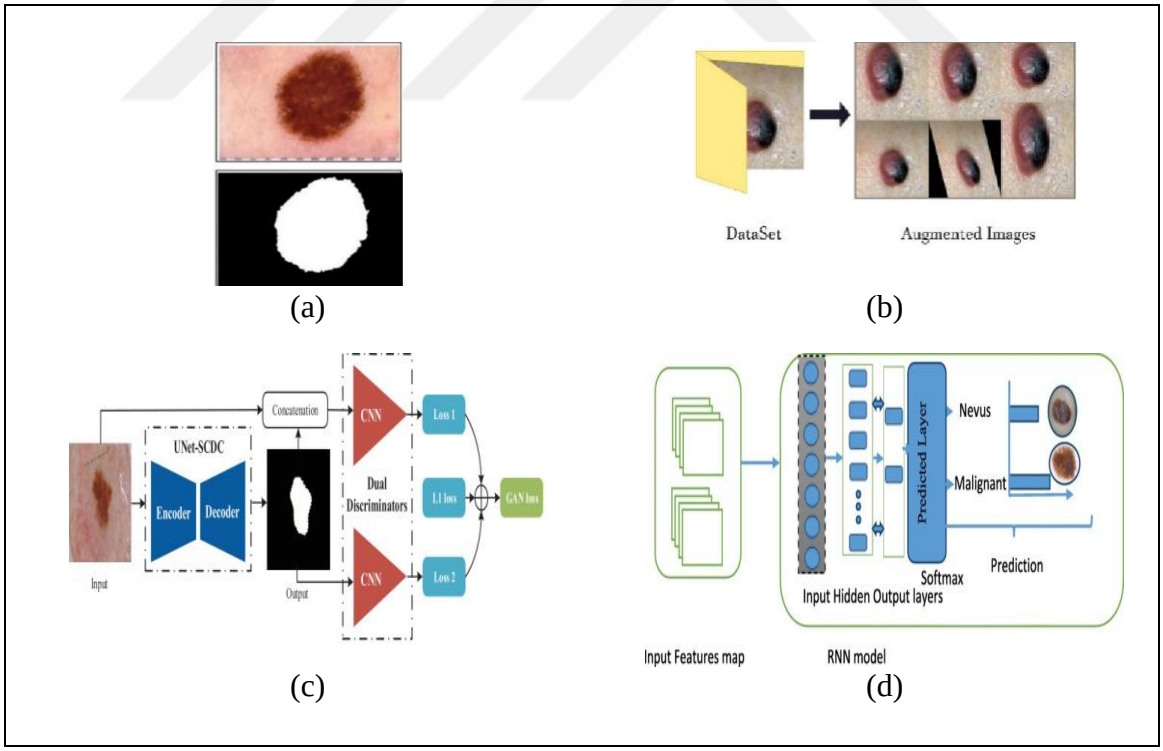

Figure 2.1: Skin Cancer Detection Techniques (A) Image Segmentation, (B) Transfer Learning, (C) Generative Adversarial Networks (Gans), (D) Recurrent Neural Networks (Rnns).

2.2 AUTOMATIC SKIN CANCER DETECTION METHODS

The increased incidence of the illness has made automated skin cancer detection systems more and more crucial in recent years. These methods rely on image analysis algorithms and advanced machine-learning techniques to accurately and quickly identify and analyze skin lesions, Skin cancer might be present, which could be indicated. Computer imaging is one of the most used automated approaches for finding skin cancer, dermoscopy, and automatic lesion classification. Computer imaging uses digital cameras to capture images of the skin and then uses software to analyze them. Dermoscopy is a non-invasive imaging method which uses a special microscope to examine the skin. Automatic lesion classification is a machine learning-based method that uses algorithms to classify skin lesions as benign or malignant. Automated skin cancer detection methods are invaluable for early detection, allowing for treatment to begin quickly before the disease progresses. While these methods are more accurate and faster than manual examination, they still require a trained medical professional to make the final diagnosis[22].

2.2.1 Traditional Methods

2.2.1.1. Support Vector Machines (SVM)

Support Vector Machines (SVM) are a subset of artificial intelligence that have been employed in the medical field to aid in the detection of skin cancer. SVM employs supervised learning, which means it is trained on a set of labeled data before making predictions about fresh data. The method looks for a plane or line that divides the training set's classes into two distinct groups. Images of skin lesions have been accurately classified into benign or malignant classifications using SVM. SVM has been shown to be nearly as accurate as a dermatologist at making the diagnosis of skin cancer. SVM is an excellent tool for doctors to utilize to identify skin cancer in its early stages and give patients life-saving therapy[23].

2.2.1.2. Deep Learning Methods

Deep learning is an effective tool for examining medical photographs, including those used to identify skin cancer. Images may be correctly and rapidly evaluated with the use of deep learning, enabling more precise diagnosis. Deep learning may also be used to spot early indications of skin cancer, such alterations in skin tone and texture. Deep learning may also be used to develop more efficient medicines like targeted therapies and to forecast a patient's chance of developing skin cancer again. The detection, diagnosis, and treatment of skin cancer may be revolutionized by deep learning[24].

2.2.1.3. Artificial Neural Network (ANN)

Artificial Neural Networks (ANNs) are employed in the medical industry to identify skin cancer. ANNs are effective at identifying patterns and can be employed to find malignant cells. ANNs can detect the presence of malignant cells and distinguish them from healthy cells by examining a patient's skin tissue sample. ANNs can identify skin cancer with an accuracy that is on par with a human expert. Additionally, because ANNs are unaffected by individual biases, they can offer a more objective diagnosis. Aside from skin cancer, ANNs are showing promise in the diagnosis of other diseases, including as lung and breast cancer [25].

2.2.1.4. Recurrent Neural Networks (RNN)

Recurrent neural networks (RNNs) are a form of artificial neural network that are used for time-series forecasting, voice recognition, and other sequence modeling applications. RNNs have recently been utilized to identify skin cancer. RNNs have proven they can identify patterns and learn from them. They are therefore excellent at identifying malignant tumors in pictures. Numerous studies have demonstrated that even with little training data, RNNs are highly accurate in detecting skin cancer. Inferring associations between lesions from their surroundings is another capability of RNNs. They can distinguish minute changes between benign and malignant tumours because to this. There is still considerable work to be done in order to improve the accuracy and robustness of skin cancer diagnosis, even though RNNs have showed encouraging outcomes.[26].

2.2.1.5. Convolutional Neural Network (CNN)

Convolutional Neural Networks (CNN) is a class of deep learning algorithm that is frequently employed for image identification tasks and has been effectively utilized to identify skin cancer. Finding skin lesions and distinguishing them from benign lesions have been proven to be particularly easy using CNNs. This is so that CNNs can detect minute variations in color and texture that are difficult for humans to notice. In order to discover more complicated patterns, CNNs may also be trained on a huge number of pictures. In various studies, CNNs have been used to detect skin cancer, and they appear to be more accurate than conventional approaches in doing so[27].

2.2.1.6. You Only Look Once (YOLO)

You Only Look Once (YOLO) is a new technique that can be applied to the diagnosis of skin cancer. YOLO uses a convolutional neural network to identify and name items in images and videos. A single neural network may detect several items in an image or video, according to the technology's premise. Real-time skin cancer detection in pictures and videos is possible with YOLO. Doctors and nurses may use YOLO to swiftly and precisely identify the indicators of skin cancer since it is rapid and accurate. People who have trouble recognizing and understanding indicators of skin cancer might also benefit from YOLO. YOLO can aid in the early identification and treatment of skin cancer, which can lower the skin cancer death rate[28].

2.3 SKIN CANCER DETECTION DATASETS

Skin cancer detection datasets are datasets that contain information related to the diagnosis, treatment, and prevention of skin cancer. The datasets may include medical images, patient records, clinic notes, pathology reports, and other relevant data. These datasets can be used by healthcare professionals, researchers, and data scientists to build models for skin cancer detection. They can also be used to develop new treatments and identify risk factors.

This section displays various dataset categories according to the tools and techniques used to collect them as well as the dataset type itself (images or videos). Samples of databases used to identify skin cancer include:

a. Skin Cancer MNIST:
HAM10000: This dataset contains 10015 dermatoscopic images of pigmented lesions, which can be used to train computer vision models for skin cancer detection[29].

b. Skin Lesion Analysis Towards Melanoma Detection:
This dataset consists of 2594 skin images and segmentations that can be used to train image segmentation and classification models for skin cancer detection[30].

c. ISIC Archive:
This dataset contains over 25,000 images of skin lesions that can be used to train computer vision models for skin cancer detection [31].

d. Melanoma Classification:

This dataset provides over 1 million skin images for training deep learning models for skin cancer detection. The most accurate method for skin cancer detection is UAV imagery using the local binary pattern (LBP) feature extraction and SVM classifier, which achieved an accuracy of around 97.6%[17],[32].

2.3.1 Convolutional Neural Network (CNN)

Compared to other networks that employ FC layers, Convolutional Neural Network (CNN), sometimes referred to as ConvNet, is a form of ANN with a deep feed-forward architecture and higher generalization capabilities. Faster object identification is made possible by its ability to gather highly generalized aspects of objects, notably geographic information[33].

CNN is employed in a number of computer vision applications, such as the detection of skin cancer and picture classification. It is similar to a basic neural network. Similar to neural networks, CNN also contains learnable characteristics like weights and biases., as shown in Figure 1. (Figure 2.2).

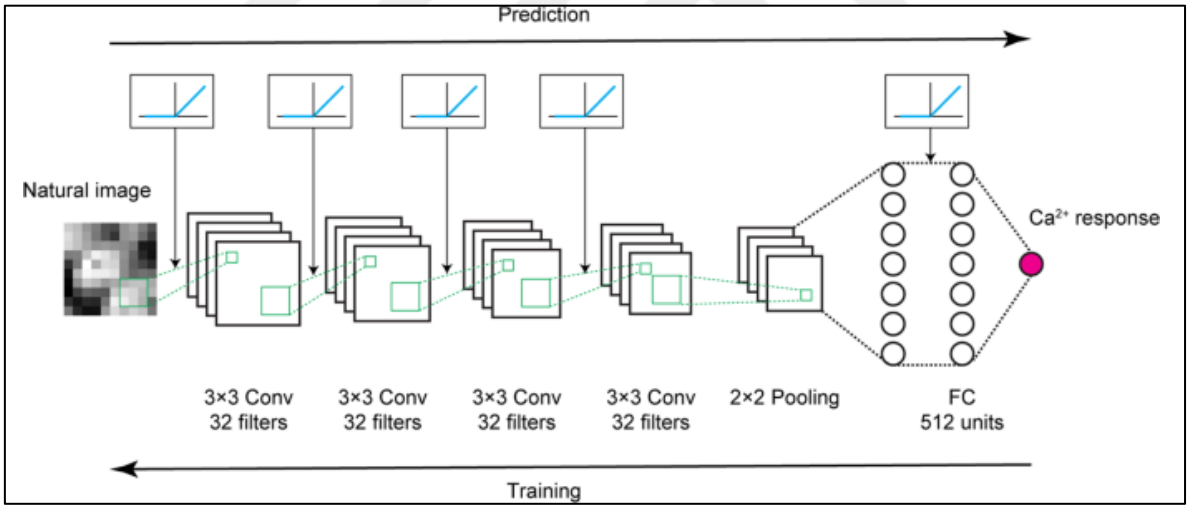

Figure 2.2 : Shows the working of Convolutional Neural Network [34].

Despite having a limited number of processing layers, the deep CNN model can learn many distinct conceptual levels from raw data (such as an image). (Such as an image). The early layers identify and extract high-level features, as opposed to the later layers, which identify and extract low-level features (at a higher level of abstraction). (With higher abstraction). Figure 2.3 depicts the basic architecture of a CNN, and the following section discusses the various types of layers in greater depth.[33].

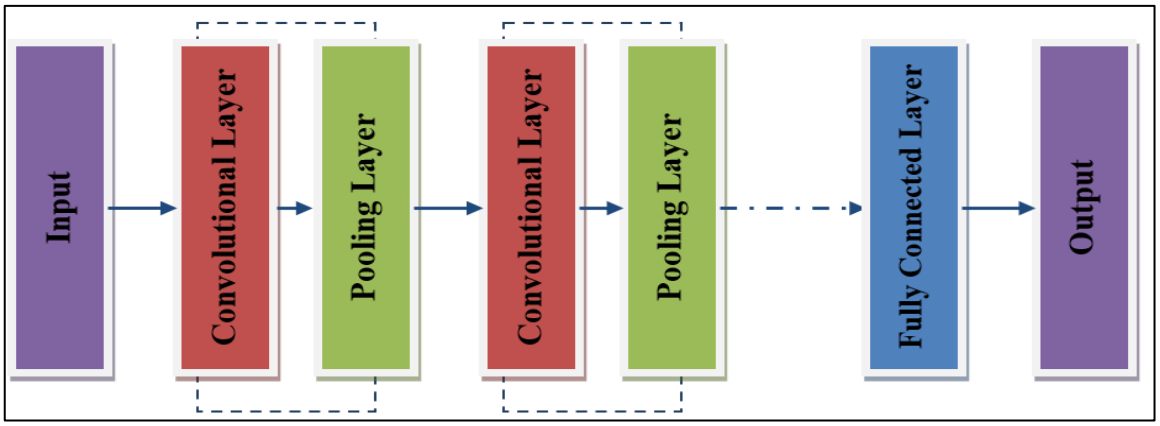

Figure 2.3: Conceptual Model of CNN.

2.3.2 Convolutional layer

The convolutional layer is an essential piece of an (CNN). This layer takes an image with N-dimensions as input and uses a set of convolution filters to do a convolution on it. These filters, also known as kernels, analyze each pixel in the image to determine whether various features, such as edges, are present. These kernels usually have sizes between 3x3, 5x5, and 7x7, and are designed to detect certain features with trained weights. The likelihood that a specific characteristic is present is determined by the convolutional operation, which is the product and total of two matrices element-by-element. Figure 2.4 illustrates this process with input and output frames and the kernel being used. [35].

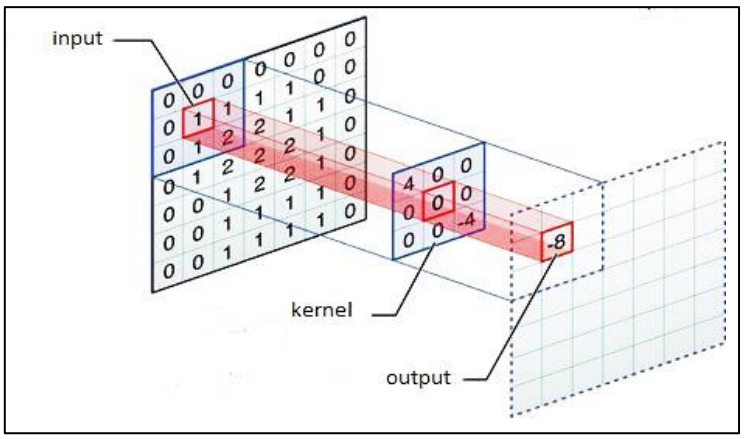

Figure 2.4: Kernel of CNN.

2.3.3 Pooling layer

After convolutional layers, CNNs typically employ pooling layer methods, sometimes referred to as subsampling or downsampling, to reduce the dimension. Strides and filter size are parameters for the pooling layer. Max pooling and average pooling, which depend on the maximum and average values, respectively, are two well-liked variations of layer pooling. Average pooling is less frequently utilized than maximum pooling. In the pooling layer, there are no parameters that must be learnt. The idea behind max pooling is that a large number denotes a high possibility of spotting a characteristic[36]. Figure shows an example of a convolution layer followed by a pooling layer. (2.5).

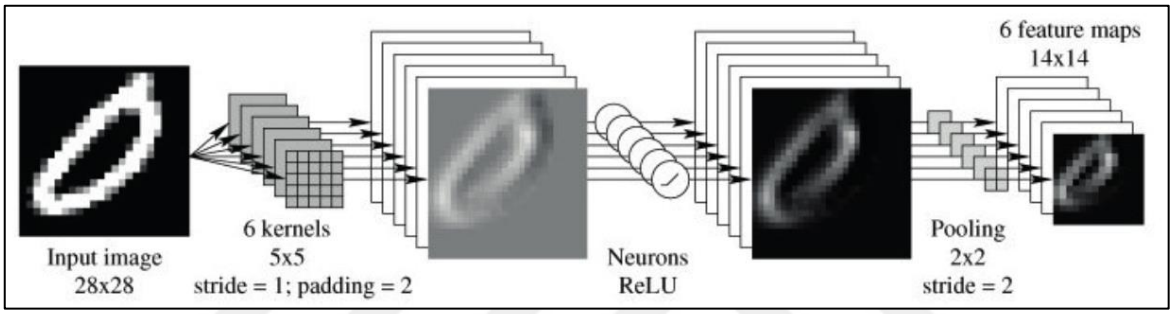

Figure 2.5: Shows the convolution layer is accompanied by the pooling layer.

Max pooling minimizes the representation size, which in turn minimizes the amount of RAM and network activities needed. The following formula can be used to determine the largest possible output quantity from a sharing operation:

$$\text{outp} = \frac{(n + 2p - f)}{s} + 1 \qquad (2.1)$$

such as:

n: numbers of filters, p: Padding amount, f: Size of filter, s: Stride

2.3.4 The layer of fully-connected

This layer is composed of neurons, weights, and biases. It is used to bridge the gap between neurons in one layer and those in the next. It allows individuals to learn how to identify images [37]. The data is converted into a feature vector, which is then inserted into the neural network in a fully-connected manner. A chance distribution for the result is generated as a result. The leveling procedure is demonstrated in (Figure 2.6).

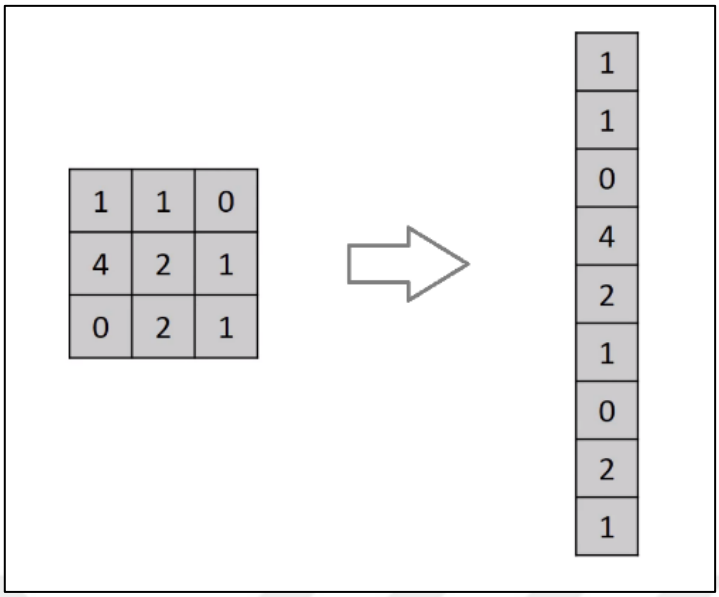

Figure 2.6: Data in The Fully-Connected Layer Being Flattened

The rows of input data are combined to create a long feature vector. This feature vector is then taken through a series of layers that are closely packed together. Each layer has its own weights and biases, and the vector is multiplied by these weights and added to the biases before being sent through a nonlinearity, as depicted in Figure (2.7).

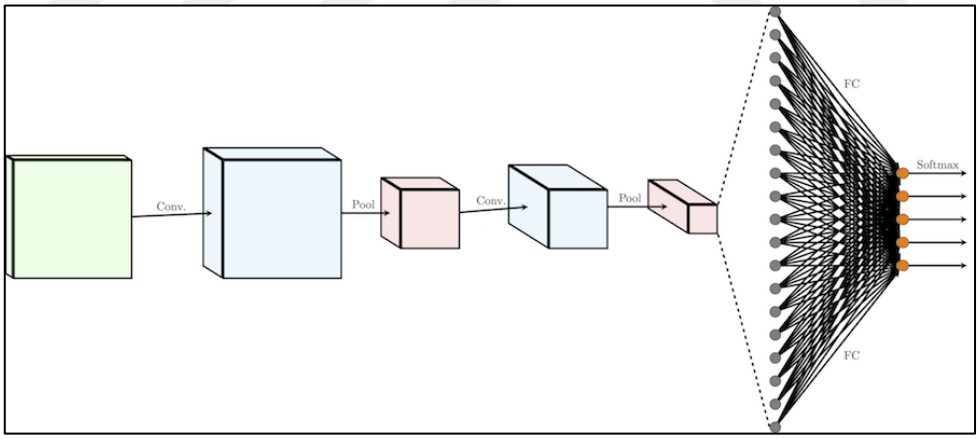

Figure 2.7: Fully-Connected layer

2.4 MODEL EVALUATION

The confusion matrix is the most enduring method for assessing the efficiency of a classification model. It enables us to check the performance of our model, recognize its flaws, and indicate changes that need to be made.

2.4.1 Matrix of Confusion

When N is the total number of target groups, a confusion matrix, which has NxN dimensions, is used to evaluate how effectively a classification method is working. This matrix compares actual goal values to predictions made by the ML model. This gives us a thorough understanding of the effectiveness of our categorization model as well as its shortcomings. For a binary classification assignment like the one in this research, this will be a 2x2 array of four values. as shown in Figure. (2.8)[38]:

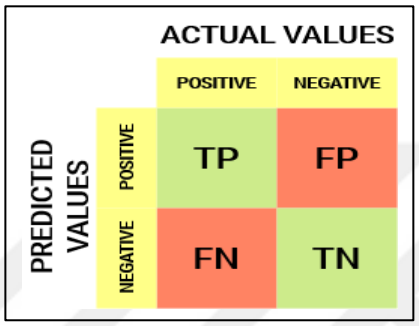

Figure 2.8: Confusion Matrix with 2 Classes

such as [39], [40]]:

True Positive (TP*)*

a. The real amount was positive, as anticipated by the algorithm, and the expected value matches the actual value.

True Negative (TN)

b. The expected value correlates to the real value.

c. The program predicted a negative value, which is what the real value was.

False Positive (FP) – Type 1 error

d. The model anticipated a positive result; however, the real outcome was negative, so the projected value was off.

False Negative (FN) – Type 2 error

e. The value was positive when the algorithm anticipated a negative value, so it was falsely forecasted.

2.4.2 Matrix of Calculate Confusion

a. Accuracy is the ratio of the total number of accurate forecasts to the total number of projections made across the complete collection, as determined by Eq (2.2) [41]]:

$$\text{accuray} = \frac{\text{TP} + \text{TN}}{\text{TP} + \text{TN} + \text{FP} + \text{FN}} \tag{2.2}$$

b. Precision, computed using Eq. (2.3), is the ratio of actual positive outcomes to all positive results that the object recognition algorithm predicts:

$$\text{Precision} = \frac{\text{TP}}{\text{TP} + \text{TN}} \tag{2.3}$$

c. Recall, computed using Eq. (2.4), is the quantity of real positive outcomes divided by the quantity of real positive outcomes.

$$\text{Recall} = \frac{\text{TP}}{\text{TP} + \text{FN}} \tag{2.4}$$

d. F1 Score: Using Eq. (2.5), the F1-Score is the harmonic mean of accuracy and memory:

$$\text{F1 Score} = \frac{2 \times (\text{precision} * \text{recall})}{(\text{precision} + \text{recall})} \tag{2.5}$$

3. THE PROPOSED SYSTEM

Skin cancer is the most common kind of cancer in people. The traditional procedures for finding skin cancer are expensive, time-consuming, and require the assistance of a qualified professional. The identification of skin cancer is aided by artificial intelligence (AI) techniques. Deep machine learning methods that use deep neural networks and computer algorithms to discover and categorize skin cancer are examples [42].

The objective of this thesis was to use AI technology to recognize, classify, locate, and characterize skin malignancies. The validity of the relationship between the scope of the data collection, the number of diagnostic classes, and the performance metrics employed to assess the models was also examined in the thesis. The methods used in this study to improve the accuracy of melanoma detection will be covered in this part.

3.1 THE PROPOSED SYSTEM

This chapter presents the salient phases of the suggested skin cancer detection method. A deep learning model is the foundation of the suggested system. The first stage was to collect the dataset required for this purpose, followed by selecting the suitable model for the process, followed by the training process, and finally the results were retrieved and analyzed. These stages will discuss in detail one by one.

3.1.1 Segmentation of the Lesion

The K-Means grouping method, dilation, masking or filtration, and thresholding are used to divide a lesion picture. The first method is used to perform the tumor segmentation.

Algorithm 1: Lesion Segmentation Input: Lesion image Output: Segmented lesion image

Step 1: Apply K-Means clustering (k=2). Step 2: Thresholding should be applied to the K-Means result. Step 3: Based on binary pictures, extract important components. Step 4: Choose the smallest component from the extracted components. Step 5: Apply dilation on the selected component. Step 6: Generate a binary mask as output. Step 7: Apply the binary mask to the original image.

3.1.2 Initial Processing

Border identification is performed using the Sobel operator, and inpainting is performed using the median filter. (specifically, finding the location of body hairs on lesions). The second method involves preprocessing split tumors.

Preprocessing Algorithm 2 segmented lesion picture as input Preprocessed lesion picture as the output

First, create a grayscale version of an RGB picture. Step 2: Apply the Sobel operator to edge recognition. Step 3: Apply a median filter to improve the statistics. 4. Perform Blob recognition. Sort the Blobs by area in step five. Apply Erosion in step six. Use a median filter and nearby images in step seven.

3.1.3 The Extraction of Features

It is standard procedure to categorize the features during feature extraction based on their texture, form, and strength. The core characteristics of texture that can be determined using the Gray Level Co-occurrence Matrix (GLCM) are correlation, contrast, energy, uniformity, and entropy values [13]. Area, perimeter, circularity, and pixel count are the form features that can be obtained. The traits derived from strength are variation and chance. An application created in Python [43] is used to determine the Local Binary Patterns (LBP) [13] and GLCM features of the tumors after they have been cut out and preprocessed.

3.1.4 Dissecting the Different Types of Lesions

The recovered traits are put into an SVM [16] classifier to determine whether a specific group of dermoscopy pictures is cancerous or benign. The standardized categorization ratings, which run from 0 (benign) to 1 (severe), are used to compute confidence intervals. (malignant).

The technical description of an SVM by a discriminative classifier is a disjoint hyperplane. Performance and precision are determined by the hyperplane cull and kernel settings. A non-probabilistic binary linear classifier called an SVM learns to categorize new cases based on a set of training samples that have been classified into one of two groups. Strong generalization ability.

3.2 SKIN CANCER DIAGNOSIS

Deep learning has shown promising results in the field of skin cancer diagnosis. Here's how it's typically done:

a. 1. Data collection: The correct diagnoses are marked on a massive dataset of dermoscopic pictures of skin lesions and healthy skin.

b. Data Preprocessing: The images are preprocessed so that they can be fed into a deep learning model. This could entail scaling the photos, standardizing the pixel values, and dividing the data into training, validation, and test sets.

c. 1. A deep learning model, such a convolutional neural network, is defined. (CNN). The model creates a diagnostic prediction from an input picture.

d. Model Training: Using supervised learning, the model is trained on annotated dermoscopic pictures. As targets, the model is given the input photos and their accompanying diagnoses. The weights of the model are adjusted to reduce the discrepancy between its predictions and the ground-truth diagnoses.

e. Model Validation: To measure the model's performance and prevent overfitting, it is evaluated on a validation set.

f. Hyperparameter tuning: To enhance the performance of the model, the learning rate, batch size, and number of epochs are all fine-tuned.

g. Model Deployment: The completed trained model can be used in clinical settings to diagnose skin cancer.

It is crucial to note that deep learning-based skin cancer detection is still in its infancy and will need additional proof of concept before being widely adopted in clinical practice. The effectiveness of deep learning models for skin cancer diagnosis can also be improved by using larger and more varied datasets and incorporating domain-specific information into the model design. The process of the suggested skin cancer detection system is depicted in Figure (3.1).

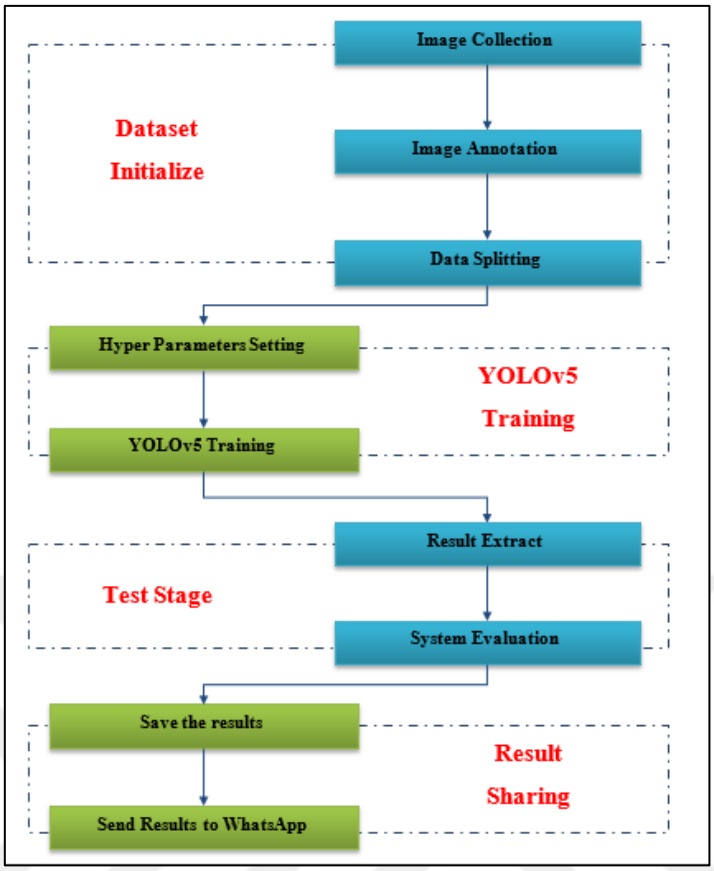

Figure 3.1: Workflow of The Proposed Skin Cancer Detection System.

3.2.1 Dataset Initialize

Four main phases make up the initialization of a skin cancer picture dataset: image collection, noise reduction pre-processing techniques, image annotation, and ultimately data separation. The main steps needed to use the dataset are shown in (Figure 3.2).

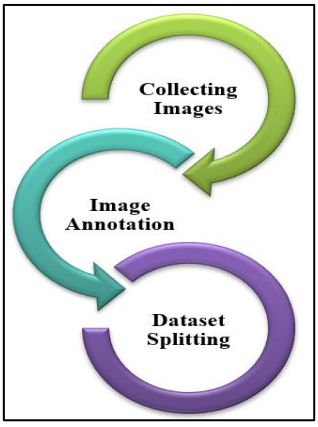

Figure 3.2: The Workflow of Dataset Initializing.

Collecting Images:

Selecting high-quality photos with distinct characteristics and more information is the first stage in selecting the required dataset, which results in better training and better results. Thus, the best skin cancer dataset that is currently available was sought after.

HAM10000 Dataset, which specializes in a variety of skin cancers, including localisation, scalp, ear, and others, was finally selected after a protracted search. 10015 dermatoscopic pictures make up the finished dataset, which may be utilized as a training set for scholarly machine learning.

Image Annotation Process

In this step, each class is assigned a class number, as mentioned in Table (3.1), which represents class numbers for each class of skin cancer. In the system, 10015 pictures have been annotated using Image Annotation Lab Software to provide a helpful ground truth for the dataset.

Table 3.1: Skin Cancer Classes and Class No.

Class	**Class No.**	**Class**	**Class No.**	**Class**	**Class No.**	**Class**	**Class No.**
localization	0	back	4	abdomen	8	neck	12
scalp	1	trunk	5	unknown	9	hand	13
ear	2	chest	6	lower extremity	10	foot	14
face	3	upper extremity	7	genital	11	acral	15

The primary steps of the annotation process are as follows:

a. Define the class labels of the desired objects, as shown in Table (3.1). • For each image, draw a Region of Interest (ROI) around the object. • Assign the class label (number) to each bounding box. • Export the annotations in YOLO format.

Each picture file stored in the same place generates a single YOLOv5-styled.txt file. Each image's comments are stored in a unique.txt file that includes details on the image's class, coordinates, and measurements.

$< object - class >< x >< y >< width >< height >$

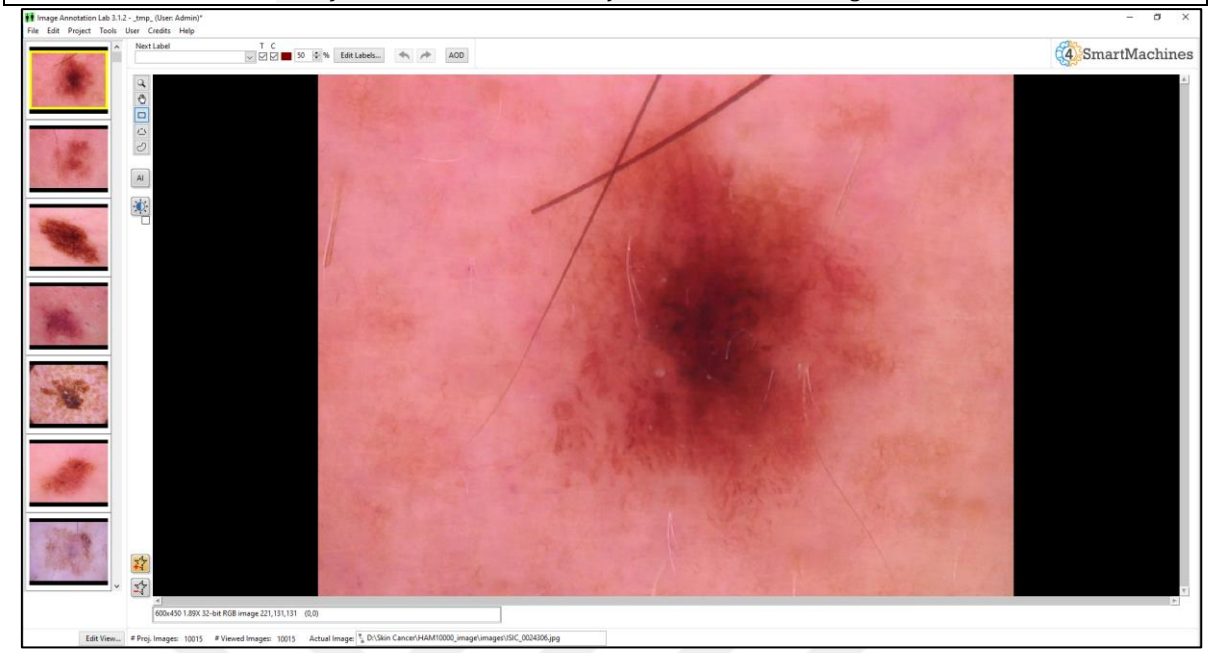

Figure 3.3: Shows the Image Annotation Lab GUI.

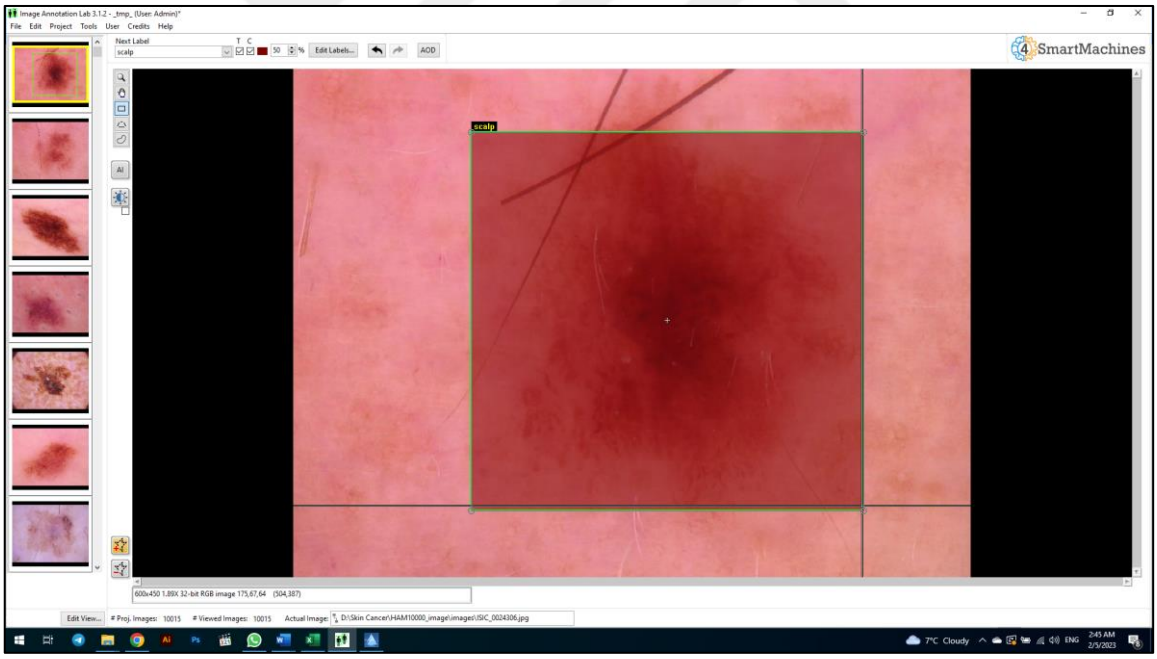

Figure 3.4: Shows the process on Annotation and selecting the appropriate class**.**

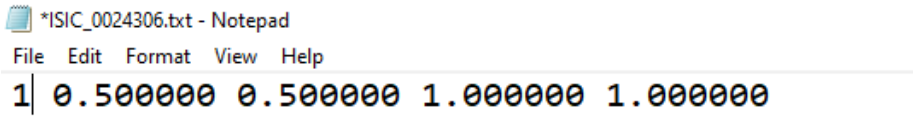

Figure 3.5: Shows the Annotation of YOLOv5 style.

3.3 COMPUTATIONAL METHODS

Since melanoma skin lesions look differently at different stages of the disease's course, analysing and classifying them is a difficult problem. Recent findings from our studies and clinical experience with melanoma early detection indicate that a new strategy for the classification process is needed to enhance identification outcomes. The fully functional version of the computer-aided diagnostic system. Each of the medical images under study undergoes a round of pre-processing and segmentation, the first two phases in the process.

The pre-processing stage is essential for enhancing image quality since distracting artifacts such skin lines, air bubbles, and hairs may be seen in almost every dermoscopic image. In the pre-processing stage, there are three algorithms:

i. Getting rid of the black frames that were added to the picture during digitization by employing the HSL lightness component.
ii. Smoothing: A Gaussian filter is used to smooth out the air bubbles and fine hairs.
iii. In order to get rid of the dark, coarse hairs, we used the white top-hat transformation for the inpainting of black hair. The pixels along the hair line are replaced with values derived from the surrounding pixels.

One of the most difficult types of pictures to segment is a medical image, yet this process is essential for analyzing and diagnosing the image in sequence. Based on the results of our study comparing various segmentation approaches, A seeded region-growing segmentation technique is used to extract skin lesions from images.

After the first two phases, the mole on the skin is segmented and then assigned to one of two different categorization methods. The molecular diameter serves as the dividing line. The Micro-Melanoma method is used for moles on the skin less than 5 mm in diameter, whereas the Specialized Melanocytic Lesion algorithm is used for larger moles. Because determining the lesion's width from a single medical photograph is impossible, the user must provide this

information. Micro melanomas make up just a small percentage of all lesions diagnosed (between 1% and 17%). Melanomas may be classified as either in situ, with a median diameter of approximately 1 cm, or invasive, with a median diameter of above 6 mm. Micro melanomas may be uncommon, yet they're the cause of most misdiagnoses. By isolating the effects of each modification, we can create a computerized diagnostic system with higher precision and reliability. There is extensive documentation for the Micro-Melanoma method and the Specialized Melanocytic Lesion algorithm in [44], [45].

3.3.1 Dataset Splitting

The ability of a deep learning system to work with unseen data is by far its most crucial component. In order to evaluate the enhanced deep learning model, the dataset was divided into training and testing datasets, as shown in Table. (3.2). Depending on the quantity of data accessible, the dataset should be divided so that neither subset is overly big.

As shown in the ratios (Training 80%: Test 20%), the information was divided into training, validation, and testing groups. (Figures 3.6 and 3.7). Python code was used for the dataset splitting procedure, which randomly divides the dataset into training and validation groups and assigns each group a certain ratio.

Table 3.2: The Split Ratio of The Dataset and The Number of Images in Each Category.

Category	**Train 64%**	**Valid 16%**	**Test 20%**	**Total**
Scalp	81	21	26	**128**
Ear	35	9	12	**56**
Face	476	120	149	**745**
Back	1402	351	439	**2192**
Trunk	898	225	281	**1404**
Chest	260	66	81	**407**
Upper extremity	715	179	224	**1118**
Abdomen	649	163	203	**1015**

Table 3.3: The Split Ratio of The Dataset and The Number of Images in Each Category."Table continued"

Unknown	149	38	47	**234**
Lower extremity	1329	333	415	**2077**
Genital	30	8	10	**48**
Neck	107	27	34	**168**
Hand	57	15	18	**90**
Foot	204	52	63	**319**
Acral	4	2	1	**7**
Total	**6396**	**1609**	**2003**	**10008**

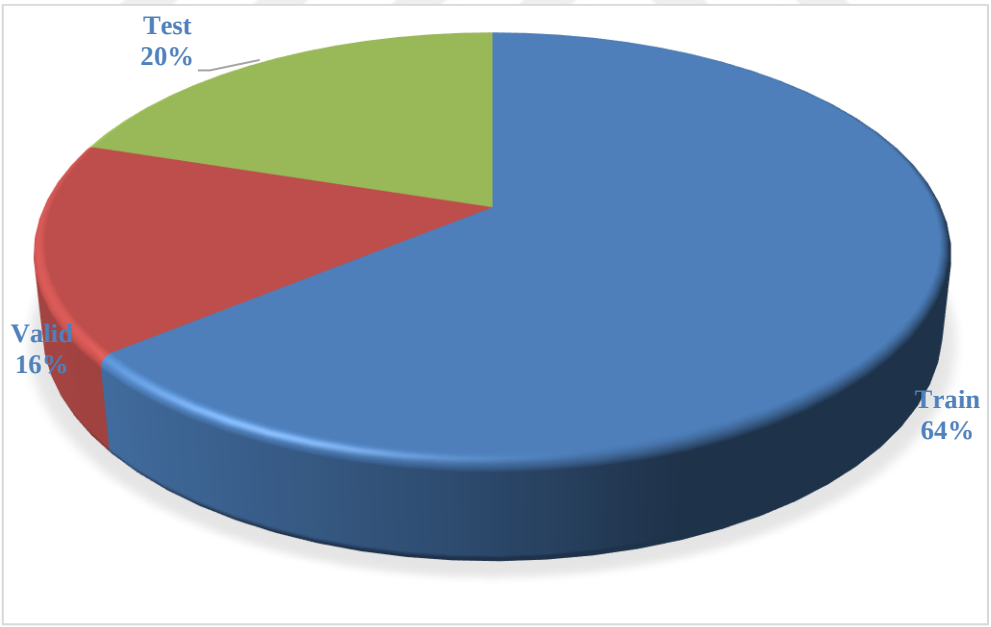

Figure 3.6: The Split ratio of the Dataset.

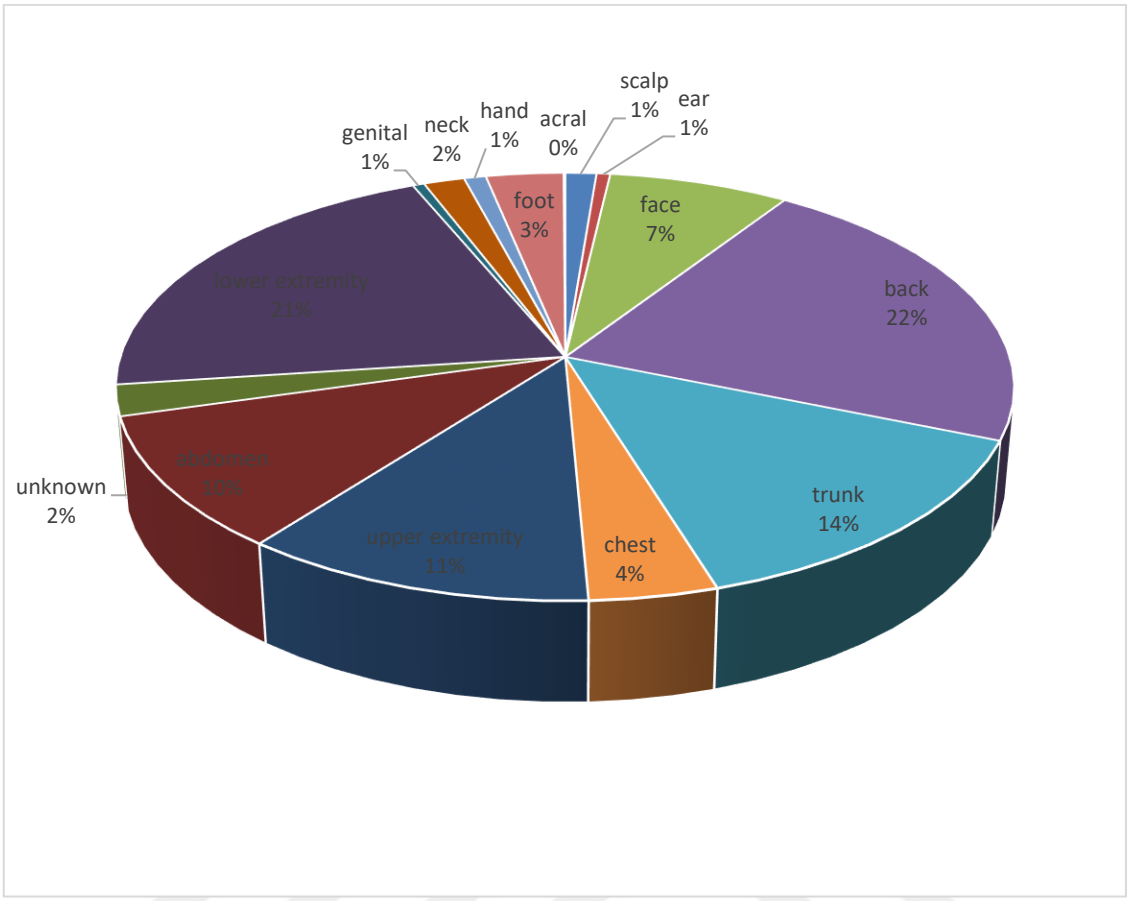

Figure 3.7: The Ratio of Each Class in The Dataset.

3.4 MODEL TRAINING

The task of skin cancer detection, specifically, is carried out on the acquired images or video sequences concerning object detection challenges that need to be addressed and managed. Due to its effectiveness and rapid learning capability, this thesis used the YOLOv5 deep learning model to perform skin cancer detection tasks. It is also commonly used to classify and recognize objects.

Although CNN-based object detectors are frequently used in suggestion systems, they can also be used to quickly recognize things in the real world with less computing power. In real-world applications, the YOLO network method grids the input picture and finds the targeted items inside each grid. The following stages must be carried out in the specified order in order to create a deep learning model:

a. Data Collection: Gather a large dataset of annotated images, indicating the location and class of objects in each image.
b. Data Pre-processing: Before training, resize the images in the training dataset to a fixed size and pre-process them to ensure they are suitable for input to the model. This may include normalizing pixel values, random flipping, and other data augmentation techniques.
c. Model Architecture: The YOLOv5 model design is a deep convolutional neural network (CNN) with several convolutional and fully connected layers. The model uses the incoming image as input and outputs a set of bounding box and class odds estimates for each object.
d. Loss Function: Calculate the difference between the model predictions and the ground truth annotations using a loss function. The loss function, which takes into consideration the confidence ratings of the bounding boxes, is created to balance the trade-off between accuracy and recall.
e. Optimization Algorithm: In order to reduce the loss function, update the model parameters using an optimization approach like stochastic gradient descent (SGD) or Adam. Based on the estimated gradients of the loss with respect to the parameters, the optimization method modifies the model parameters.
f. Regularization: Apply regularization techniques, like dropout and L2 regularization, to prevent overfitting during training.
g. Hyperparameter Tuning: In order to optimize the performance of the model, a number of hyperparameters, including learning rate, group size, and number of epochs, are used during the training process. Grid search or random search are two methods that are frequently used to locate the ideal hyperparameters.
h. Model Evaluation: Evaluate the trained model on a validation set to measure its performance. This may involve calculating metrics such as average precision, recall, and F1 score for each class and for the overall model.
i. Model Saving and Deployment: Once the model has reached the desired level of performance, it can be saved and deployed for real-time object detection.

3.4.1 Hyper Parameters Setting

a. Weights Initialization

In neural networks, weights are employed to generate a weighted sum of the inputs. Is utilized before training neural network models on a dataset to decide the initial values for the parameters.

b. Batch Size Control

The batch size parameter is an important hyperparameter in modern deep learning networks that must be adjusted. Because Graphic Processing Unit (GPU) parallelism allows for computational speedups, practitioners typically want to train their model with a larger batch size. During the training phase, the batch size has a significant impact. The results of the experiments show that the number of images used in training mode, the number of repeats, and the type of hardware being used are the main determinants of choosing the appropriate batch size. Larger batch sizes made possible by the GPU allow for quicker and more precise training.

With a batch size of 4, the training dataset's 10008 images will be divided into 2501 batches for each training and valid epoch.

c. Image Size

Prior to training the model, the input images should be ready by having their sizes adjusted to a suitable uniform size. Longer training times are needed for high-resolution photos. However, because they can be divided into 32 equal parts by the grid size, smaller images will train considerably more quickly, and the network may even converge more quickly.

d. Dataset

To achieve the best trained model for an object detection task, the dataset used should be as large and diverse as possible, containing a wide range of samples of the desired object. Ideally, the number of images per class should exceed 1500, and the variety of images should be representative of the real-world environment. To enhance the model's applicability, include images from various sources (such as internet-scraped images, locally collected images, and images from different cameras), taken at different times of the day, in various seasons, and under various weather, lighting, and angle conditions. Additionally, label consistency is crucial: each instance in the class should be accurately labeled.

e. Epochs Number

As a starting point, use 150 epochs. Reduce the epoch count if you see that this starts overfitting too soon. After 150 training epochs, there is still no indication of overfitting, thus the training is maintained for 300, 450, 600, etc.

3.4.2 YOLOv5 Model Training

The YOLOv5 model is trained using supervised learning, where the model is given annotated images as input and corresponding object annotations as the target output. The training process can be summarized in the following steps:

a. The model takes an input image and generates a set of predictions for bounding boxes and class probabilities for each object in the image.
b. The predicted bounding boxes and class probabilities are compared to the ground-truth annotations for the image.
c. A loss function is employed to quantify the difference between the model predictions and the ground-truth annotations.
d. The gradients of the loss concerning the model parameters are computed using backpropagation.
e. To reduce the loss, an optimization method like stochastic gradient descent (SGD) is used to change the model parameters.
f. The process is repeated for numerous epochs, where an epoch is defined as a complete pass through the training data.
g. The trained model is assessed on a validation set to measure its performance and prevent overfitting.
h. The training process continues until the model attains the desired performance on the validation set.

Dataset Image Input

YOLOv5 begins by using a picture with a uniform size of 512512 as input from the annotated dataset.

Image split into a matrix

An image is first grid-divided into 32x32 rectangles when it is put into the system. Image localization and classification are done on each grid. The enclosing areas and class odds for the items contained in them are then estimated by YOLO.

It must supply labelled data to train the model. The image has been divided into 32 by 32 grids, with Fire and No Fire classes. As a result, each grid cell's label y will be a seven-dimensional vector. The image grid and attributes are depicted in (Figure 3.8).

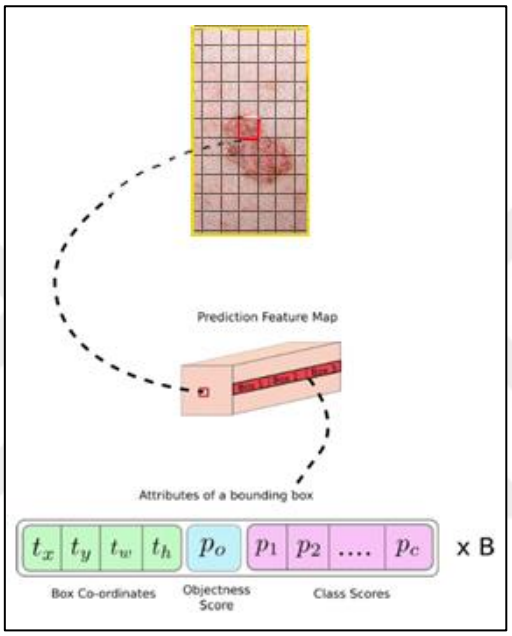

Figure 3.8: Image Grid with Characteristics.

To create a speed benchmark, the system will train with the default settings first. Various tests are then conducted to determine the best parameters to get the best outcomes. The default basic training circumstances are shown in table (3.3).

Table 3.4: Standard Conditions of Basic Training

Hyperparameters	Setting
Epoch	1000 epochs
Image Size	512 × 512
Batch Size	4
Learning Rate	0.01
Convolution layers Number	32
Filter size	3 × 3
Activation function used	SiLU
Optimizer	SGD
Cost function	BCE

3.5 THE EVALUATION OF MODEL

There are a variety of techniques for determining whether your categorization model is effective, but none have remained as effective as the confusion matrix. It enables us to evaluate the model's performance, spot defects, and offer suggestions for course correction.

3.5.1 The Matrix of Confusion

By creating a "confusion matrix," which is a NN matrix where N is the total number of categories being taken into account, one can assess the effectiveness of a categorization model. The matrix shows how predictable the ML model is in comparison to actual data. This gives it the ability to evaluate the effectiveness of the classification system and the issues it is encountering. The 22 four value arrays needed to designate binary categories. Confusion Matrix can be computed using the following methods:

a. To calculate accuracy, we divide the number of events that were successfully predicted by the total number of predictions using Eq. (3.1):

$$\text{accuray} = \frac{\text{TP+TN}}{\text{TP+TN+FP+FN}} \tag{3.2}$$

b. The object detection model's real positives to all expected positives ratio, as determined by Eq. (3.2).

$$\text{Precision} = \frac{\text{TP}}{\text{TP+TN}} \tag{3.3}$$

c. The Eq. (3.3) describes it as the product of the real positive outcome number and the genuine positive outcome number:

$$\text{Recall} = \frac{\text{TP}}{\text{TP} + \text{FN}} \tag{3.4}$$

3.5.2 Data Sharing

For the purpose of integrating the system, and after conducting network training and testing, the system was integrated by sending the results (image and diagnosis) to the concerned authorities (whether a patient or a doctor), by creating an interface containing a list of names and phone numbers of the people concerned, and by selecting One of them is sending information via WhatsApp program.

This process was carried out by implementing programming via Python, and the permissions for the WhatsApp program were made to do the necessary for that.

3.5.3 Tele dermatology for patient-doctor communication

Numerous studies [6], [46]–[48] have demonstrated the effectiveness of asynchronous Teledermatology (TD). The use of TD in dermatological clinics worldwide has significantly increased since the pandemic. Farshchian et al [49].

Skin disorders like psoriasis [6, [46]-[48], acne [46], [50], oncodermatology [51], [52], juvenile hemangiomas, hair problems [53], [47] are frequently treated with asynchronous TD. A triage strategy based on clinical pictures that is used in asynchronous TD to handle common dermatological diseases lessens the need for pointless face-to-face meetings [46], [52]. Only 15% of instances involving prevalent ambulatory dermatoses required conversion to face-to-face assessments; 84% of diagnoses and treatments were finished using TD.

McDonald et al. [54] triaged TD appointments using qualified medical photography; the outcomes showed a discharge rate of 35.1%, a conversion rate to in-person appointments of

43.8%, and a scheduling rate for therapies of 20.2%. When a dermatologist suspected skin cancer, the results of the histopathology examination agreed 72% of the time with the triage diagnosis. However, a bad picture can make a clinical evaluation difficult. Only 31.3% of all TD evaluations were changed to in-person meetings, according to Cartron et al.'s [55] research, which showed that only 50% of the pictures used for asynchronous TD were of outstanding quality.

Dermoscopy-assisted TD has been utilized in photo-triage settings. McCrary et al. reported that diagnostic accuracy increased from 45.3% to 53.6% when dermoscopic images were used in TD consultations. The most significant improvement was observed in the diagnosis of malignant skin lesions.

TD has been successfully used in the COVID-19 epidemic. According to Skayem et al. [6], following the caution about cutaneous involvement in COVID-19 infection, the average number of TD visits per day in France rose from 9.28 to 36.4. By utilizing TD, unnecessary in-person talks were decreased, saving important personal protective equipment. (PPE). TD was also used to treat patients with skin cancer and cancer linked to the dermatologist. Through asynchronous TD, patients suspected of having melanoma were triaged and managed. The precision of surgical removal was 53%, which was comparable to the pre-pandemic incidence of 56%.

4. RUSTLES AND DISSECTION

In this chapter, we examine the outcomes of the experiments done to verify the reliability of the proposed system. In section 4.2, we discussed the apparatus used in the experiments. Next, in the following part, we detail every experiment that was conducted to arrive at these conclusions on the enhancements to YOLOv5 (4.3).

4.1 EXPERIMENTAL SETUP

The relevant details regarding the experimental setup are presented here. Details on the platforms, datasets, and programs that were used are included.

4.1.1 Platforms

Listed below are some of the features of the platform that was utilized to train the algorithm:

f. Type: Laptop
g. Video Processor: RTX 3050 4 GB
h. Microarchitecture: Ryzen 5
i. Storage: 16 GB
j. Version 10 of Windows Operating System

4.1.2 Dataset

The International Skin Imaging Collaboration (ISIC) Archive, a helpful tool, is maintained by the International Society for Digital Imaging of the Skin. (ISDIS). It continues to hold the distinction for having the largest and most complete collection of top-notch dermoscopic pictures of skin lesions that is freely accessible. Researchers get access to a sizable population through the ISIC Archive, which is essential for developing and evaluating skin lesion analysis algorithms.

A typical ISIC Archive collection of malignant and benign skin lesions consists of 900 annotated dermoscopic photographs for training and 380 images for testing. The format of these pictures is 8-bit RGB. [56], which provides specialists and academics working on algorithms for the detection and classification of skin cancer with high-quality visual data.

By using the ISIC Archive, researchers can develop, test, and improve machine learning and deep learning models for skin lesion analysis, ultimately leading to better diagnostic tools

and improved patient outcomes. The ISIC Archive is continually updated, ensuring that researchers have access to the latest data for their projects.

4.1.3 Programming Language

Python's flexibility makes it an attractive choice for programmers. In the eyes of most programmers, it is the best platform for creating AI, ML, and DL projects. Python is popular for ML projects due to its extensive library of ML-specific modules. In addition to a fast code-checking process, the syntax is user-friendly and simple to grasp.

4.1.4 Programs

PyTorch 1.9 with Torchvision 0.11.0, CUDA 10.2, and the most up-to-date version of the Python library were all necessary to build the suggested system on both systems. The dataset annotation was performed in Image Annotation Lab, while image processing was handled by FastStone Photo Resizer on the platform.

4.1.5 Required Platform Installation

Python is the language utilized, and Pycharm is the platform used to execute Python commands, therefore their installation is the kernel for getting started with system programming and producing code. Following that, the Anaconda3 package is used to install the system libraries. This package is the primary backer for many of Python's standard library modules.

4.1.6 GUI (Graphic User Interface)

Although there are a number of GUI frameworks available for Python, only Tkinter is included with the language. Using Tkinter has several advantages. It works with a wide range of OSes, including Windows, Linux, and Mac OS X. Tkinter programs use native OS features to render graphical elements, making them look and feel at home on the platform where they are run.

A graphical user interface based on clicking rather than programming instructions, as in programming languages, was created for the interface to make using the software easier and more efficient. As seen in (Figure 4.1), four keys were implemented to achieve this goal and make the complete system's operation simpler.

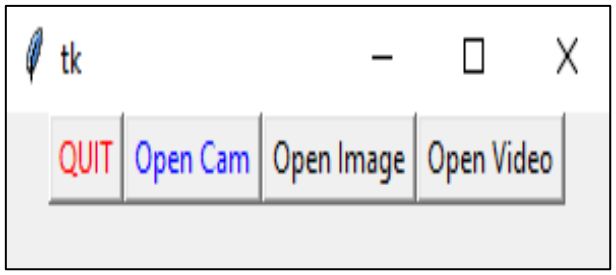

Figure 4.1: GUI of The Proposed System.

a. The "Quit," which means to shut down the system promptly and permanently.
b. The "Open Cam" activates the camera and begins processing in real time.
c. Third, click "Open Image," which will bring up a box where you may choose photographs for identification and fire detection.
d. When you press the fourth button, a window will pop up where you can choose the videos that need to be analyzed for identification and smoke detection.

4.2 EXPERIMENTAL TESTS

Experiments were conducted on a laptop running the YOLOv5 model without first conducting a test phase to validate the system and verify the algorithm's proper functioning.

Experiment No. (1)

As a first stage, we evaluated the system's efficacy using an estimated 502 skin cancer photos split into two sets of data (Train: 412, Valid: 90). The following were the outcomes of the experiment performed on a computer with minimal hardware requirements, namely the CPU, as shown in (Figure 4.2):

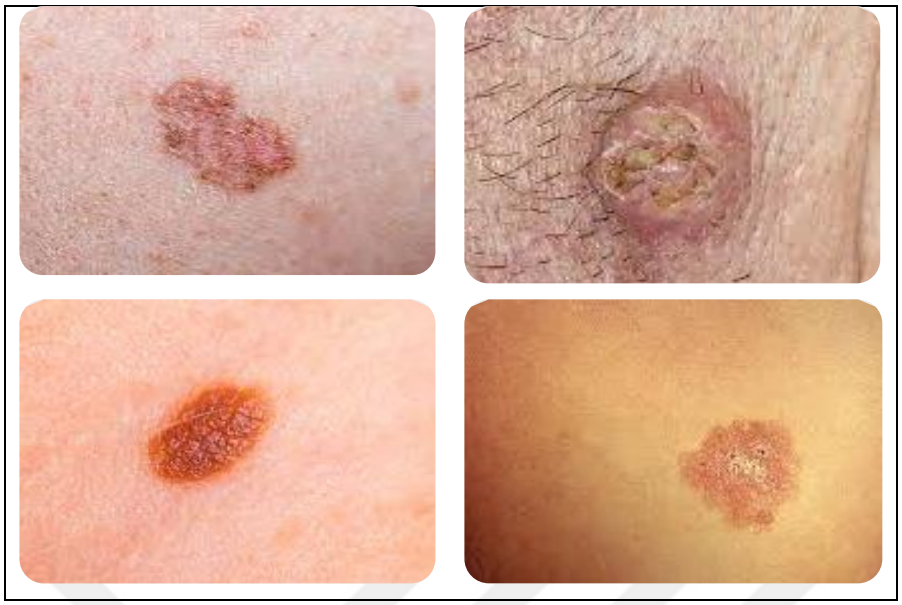

Figure 4.2: A Sample of The Dataset Used in The First Experiment

These are the experimental training hyperparameters:

Table 4.1: The Parameter Set at The Beginning of The First Experiment's Hyperparameter.

Train Images	412 Images
Valid Images	90 Images
Test Images	0 Images
Image Size	600 × 600
Train Time	28 Hours
Batch Size	4
Filter Size	3 × 3
Parameters	7199615

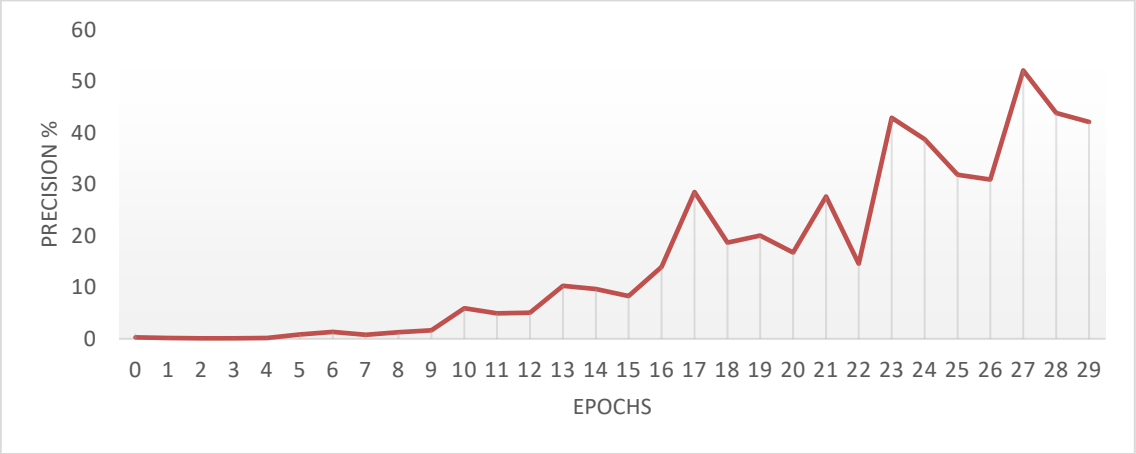

(a) the percentage of Precision

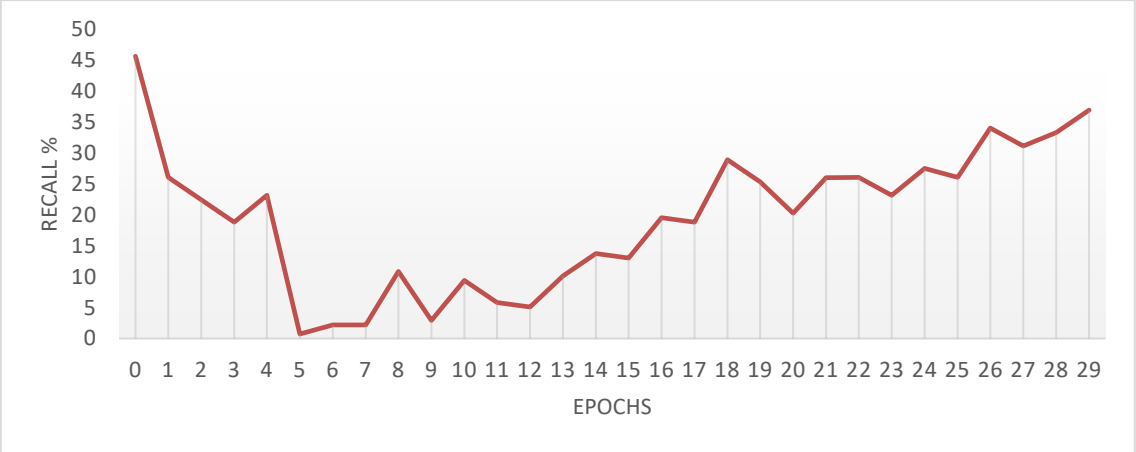

(b) the percentage of Recall

Figure 4.3: First Experiment Training Results.

As shown in (Figure 4.3), the experiment did not provide desirable results; hence, more photos needed to be collected and used in the next experiment so that the neural network could function properly.

There is a conspicuous lack of epochs in this experiment, and other studies have shown that adding more epochs improves both training and accuracy, hence this study was ultimately rejected.

Experiment No. (2)

Given that the previous experiment's dataset was too small to be useful, this one employed around 2105 (Train: 1684, Valid: 421) photos to get good results. In the end, the scholar was compelled to work on artificial intelligence using a machine that met the strict requirements outlined in section (4.1.1), and better results were obtained than the first time around by using more data, as shown in Despite the fact that the training phase was challenging and consumed a lot of the CPU's time, the researcher was forced to use a computer. (Figure 4.4).

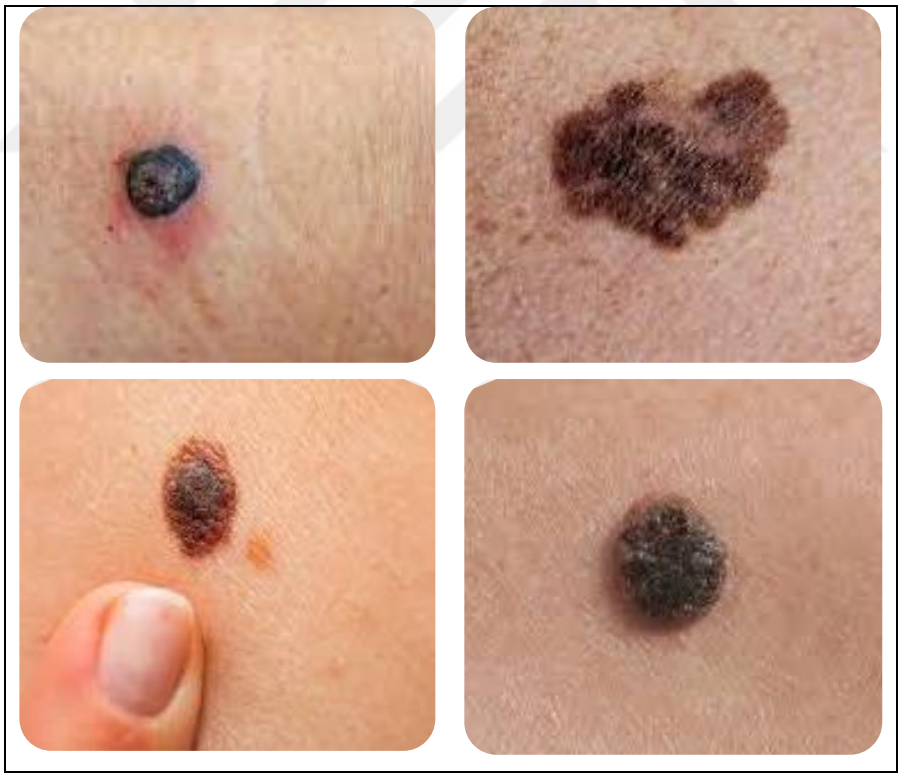

Figure 4.4: Dataset Used in The Second Experiment as An Example**.**

These were the hypermeters used in the experiment:

Table 4.2: First Value of The Second Experiment's Hyperparameter.

Train Images	1684 Images
Valid Images	421 Images
Test Images	0 Images
Image Size	600 × 600
Train Time	9 Hours
Batch Size	8
Filter Size	3 × 3
Parameters	7199615

This experiment proved without a reasonable doubt that utilizing the GPU is quicker than using the CPU, despite the fact that it used a far larger number of photos than the previous experiment.

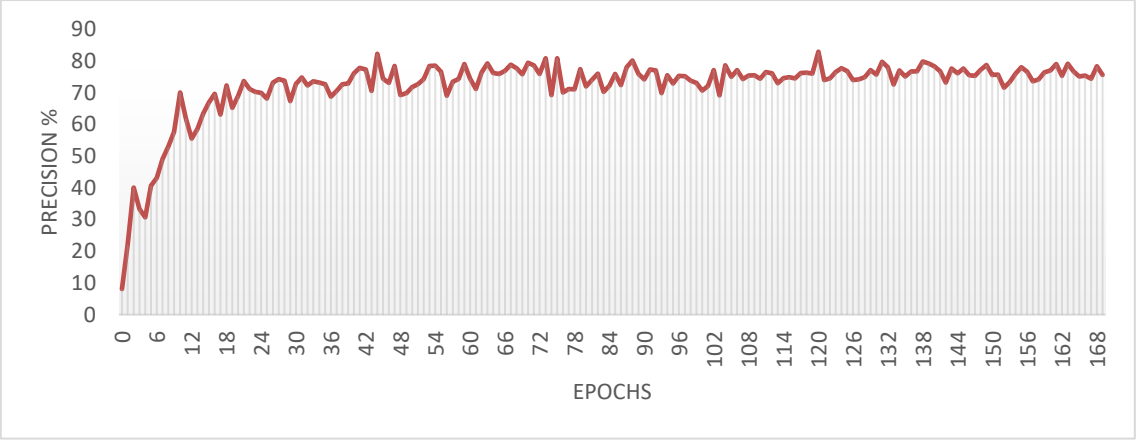

(a) the percentage of Precision %

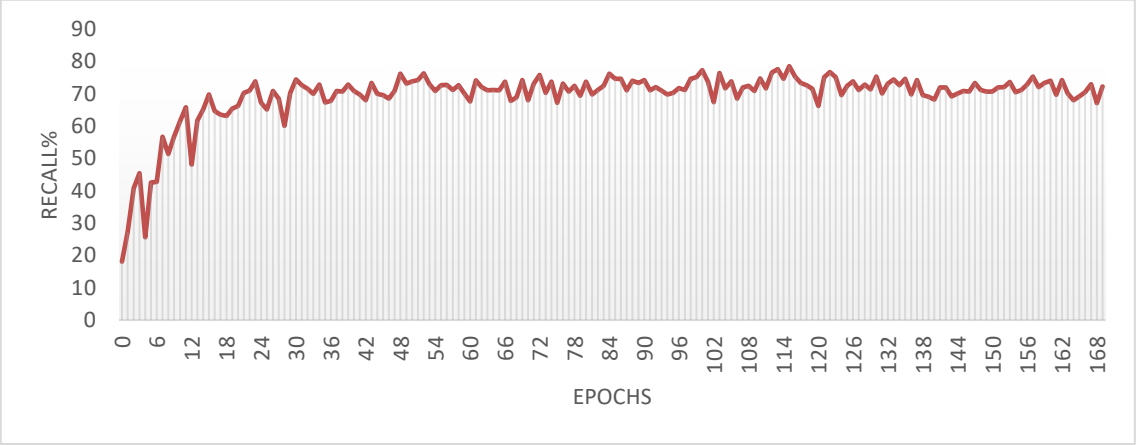

(b) the percentage of Recall

Figure 4.5: Shows the Training Results of the Second Experiment.

Experiment no. (3)

The same dataset was utilized in this experiment, but the picture size was shrunk to (224 px) to shorten the training period, the batch size was raised to 32, and the initial weight was set to 1. (YOLOV5S.pt).

Table 4.3: Third Experiment's First Hyperparameter.

Train Images	1684 Images
Valid Images	421 Images
Test Images	0 Images
Image Size	224 × 224
Train Time	2 Hours
Batch Size	32
Filter Size	3 × 3
Parameters	7199615

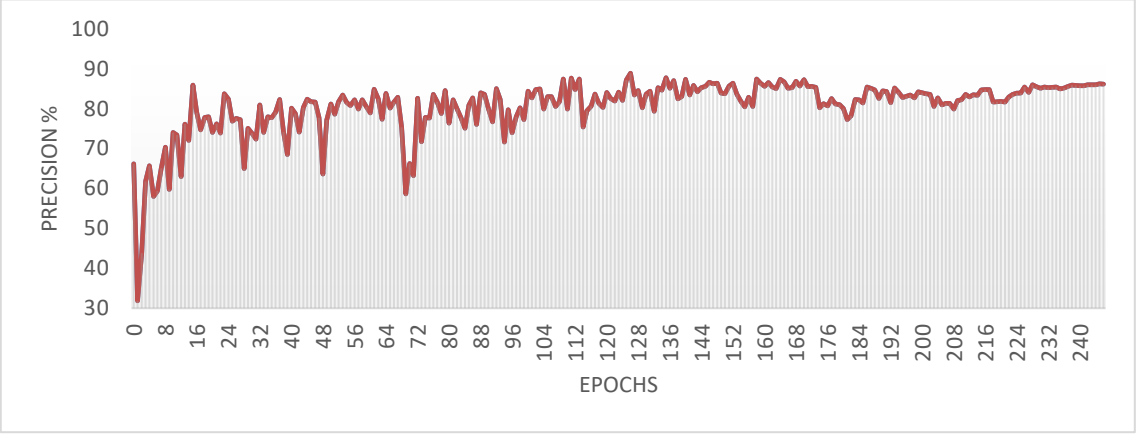

(a) the percentage of Precision %

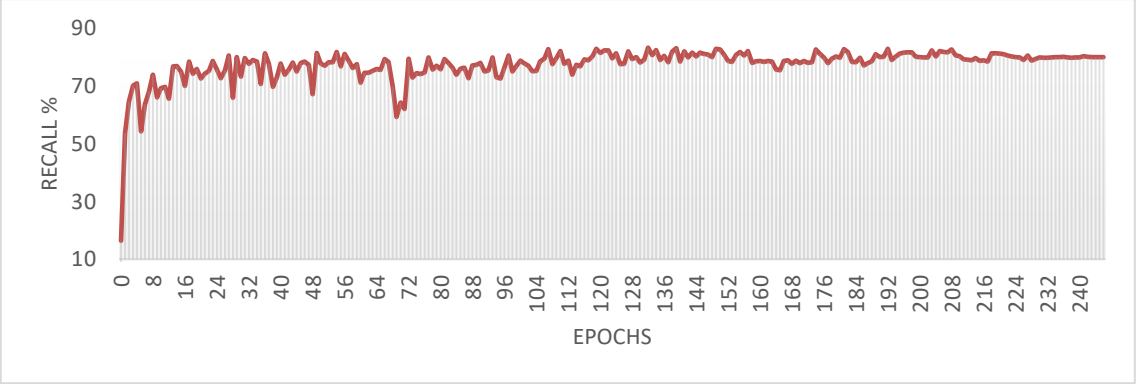

(b) the percentage of Recall

Figure 4.6: Shows the outcomes of the Third Training Experiment.

In this experiment, we examine how batch size influences the pace of training. The purpose of this study was to provide preliminary data on the impact of different batch sizes. The machine learning community is aware of how challenging it is to generalize about the impact of hyperparameters due to the considerable variation in behavior across datasets and models. We found that by decreasing picture size, we could increase batch size, resulting in more epochs with less total training time.

4.3 TEST PHASE:

After the experiments have been run on the weights that were taken from the training data, the findings will be displayed here. In addition to a detailed analysis of the experiment's accuracy and correct and wrong frames, the time required for each frame will be shown in table (4.4). In (Figure 4.7), we have an illustration of the findings obtained in the test category of the dataset.

Table 4.4: Confusion matrix results for YOLOv3.

		Actual Values	
		Positives	**Negatives**
Predicated Values	**Positives**	**676**	**11**
	Negatives	**14**	**673**

Table 4.5: Test phase results for YOLOv3.

Test Time	**pre-process (ms)**	0.2
	Inference (ms)	13.2
	NMS per image (ms)	0.9
Accuracy		98.18%
Recall		97.97%
Specificity		98.39%
Precision		98.40%
F1 Score		98.18%

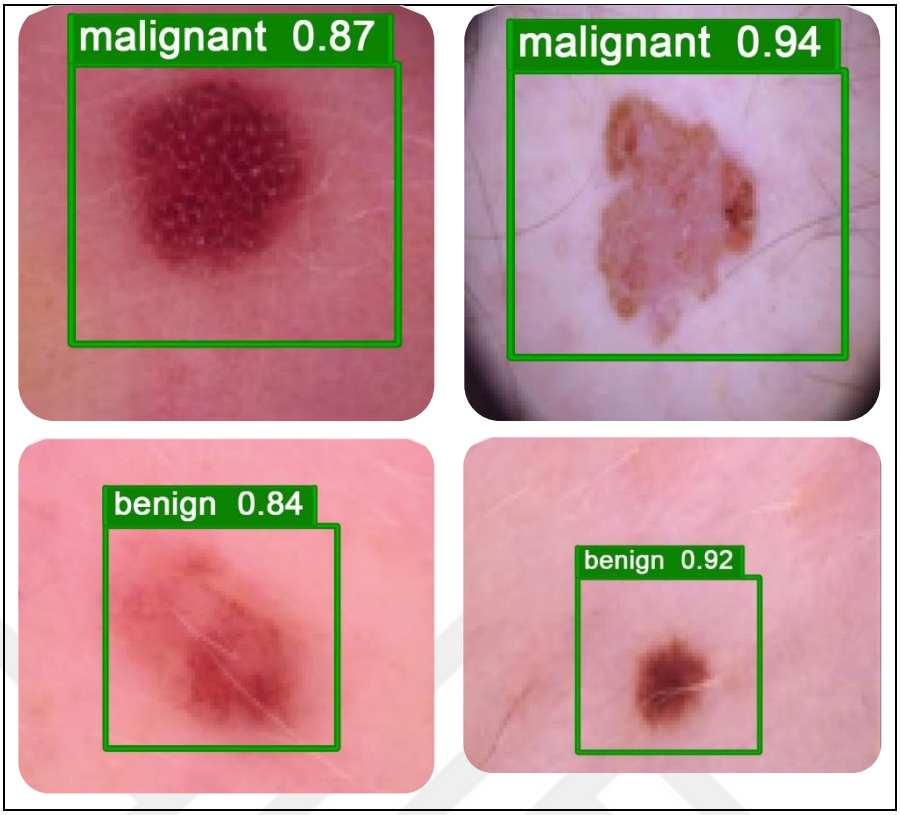

Figure 4.7: Shows The Results of Yolov3 Test For Both Malignant and Benign.

4.3.1 Segmentation of the Lesion

The finished image is the result of segmenting the original skin lesion image using K-means. The lesion image and the K-means segmentation result produced by our algorithm are shown together in (Figure 4.8). The Jaccard index values are used to assess how close the segmentation findings are to the actual photographs of skin lesions. The figures include 0.850 and 0.750, among others.

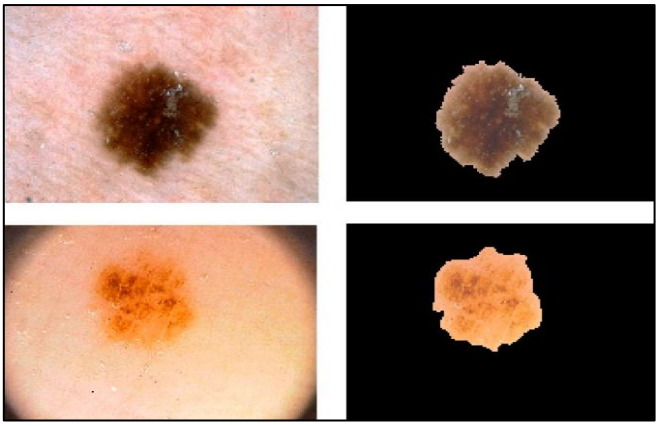

Figure 4.8: The Segmentation Stage**.**

4.3.2 Pre-processing Step

The segmented images are then passed to preprocessing. The end products are segmented and preprocessed grayscale copies of the source skin lesion images. The results of the preparation on the ISIC Archive dataset's cutaneous lesion are displayed in (Figure 4.9).

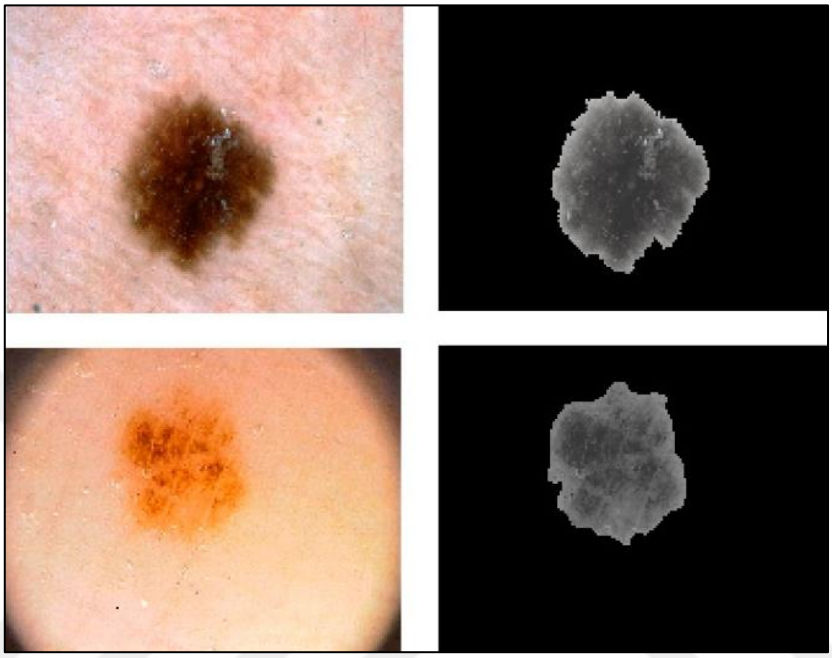

Figure 4.9: Shows the Pre-Processing Stage**.**

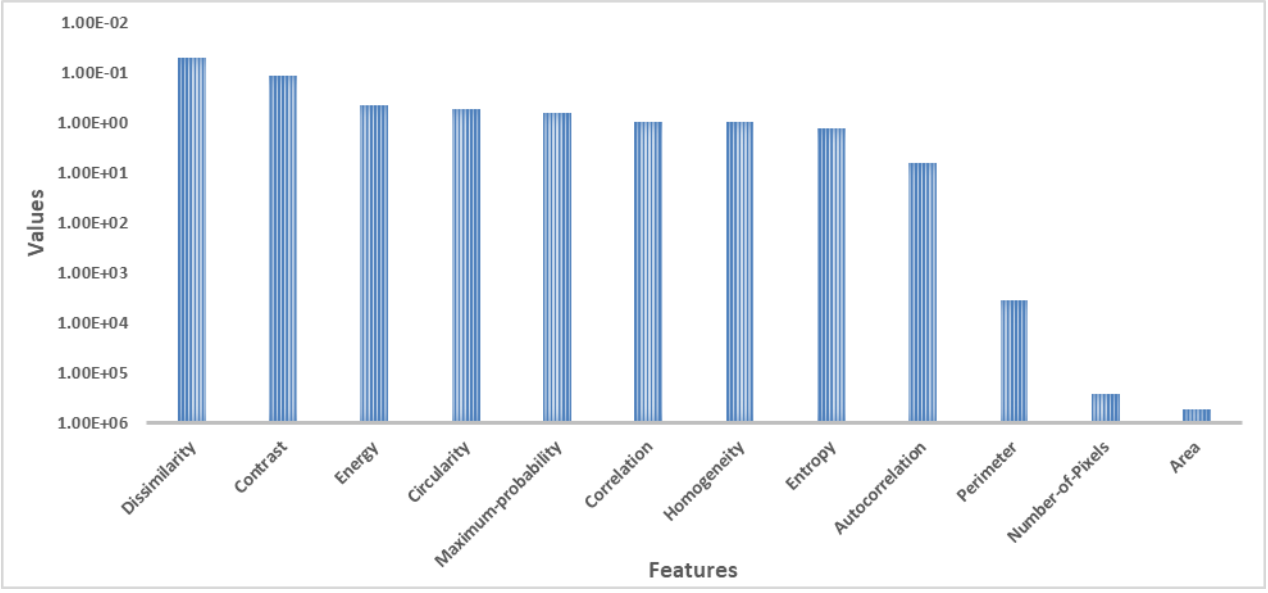

Figure 4.10: Illustrates the Values of Features Extraction.

4.3.3 Characteristics Extraction Procedure

To derive features from segmented and preprocessed lesion pictures, LBP (Local Binary Patterns) and GLCM (Gray Level Co-occurrence Matrix) features are merged. We can identify the texture, form, and intensity details of the tumors using GLCM and LBP. These feature extraction techniques help in capturing the essential patterns and details within the lesion images, which can then be used to classify and differentiate between various types of skin lesions.

The extracted LBP feature values include the following: 4.32E-02, 4.62E-02, 7.50E-02, 9.28E-02, 1.81E-01, 1.94E-01, and 9.54E-01. These values represent the distribution and frequency of various patterns present in the lesion image, which can be indicative of the lesion type and severity.

The values of the retrieved features, including both GLCM and LBP features, are illustrated in (Figure 4.10). This figure provides a visual representation of the extracted features, which can be helpful in understanding the underlying patterns and structures within the lesion images. By analyzing these features, researchers and practitioners can develop more accurate and efficient classification models for skin cancer detection and diagnosis.

4.3.4 Subtype Evolution and Classification of Lesions

When the feature extraction values are fed into the classifier for learning, the SVM (Support Vector Machine) classifier is taught to differentiate between benign and malignant skin lesions based on the input features. The provided ISIC collection contains 900 images of benign and malignant skin lesions. The remaining 30% (270 images) are used to assess the success of the classifier, while the remaining 70% (630 images) are used for training purposes.

After the SVM classifier has been trained, the test collection of input images can be used to assess it. Each image in the test group is either innocuous (representing a value of "0") or malignant (representing a value of "1"). (Representing a value of "1"). (Representing a value of "1"). Performance measures are calculated based on the four possible outcomes and used to evaluate the classifier's performance.:

a. True Positives (TP): The number of malignant lesions correctly identified as malignant by the classifier.
b. True Negatives (TN): The number of benign lesions correctly identified as benign by the classifier.
c. False Positives (FP): The number of benign lesions incorrectly identified as malignant by the classifier.
d. False Negatives (FN): The number of malignant lesions incorrectly identified as benign by the classifier.

Based on these outcomes, various performance metrics can be calculated, such as accuracy, precision, recall, and F1-score, to evaluate the classifier's effectiveness in differentiating between benign and malignant skin lesions. These metrics provide insights into the classifier's performance and can be used to fine-tune the model or compare it with other classifiers.

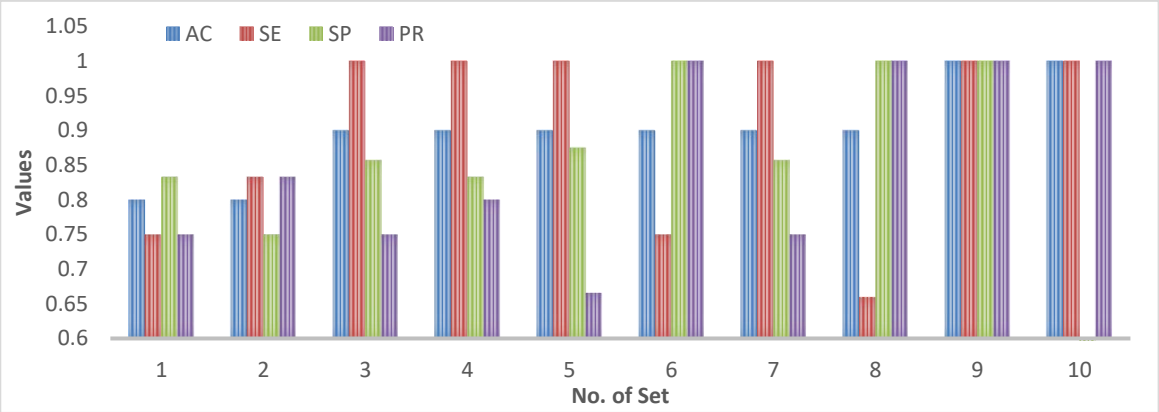

Figure 4.11: Shows The Test Results for Ten Different Image Collections**.**

Figure 4.11 displays the performance metrics for ten distinct test image collections, each of which included ten images with benign and malignant origins. Test picture group No. 10 contains just one instance—a cancerous one. The average performance metrics for this classification system are calculated using the formulas Accuracy (AC), Sensitivity (SE), Specificity (SP), and Precision. (PREC):

a. Accuracy (AC): Measures the proportion of true results (both true positives and true negatives) among the total number of cases examined. In this case, the average accuracy is 93.28%.

AC = (TP + TN) / (TP + FP + TN + FN) = 93.28%

b. Sensitivity (SE): Measures the proportion of true positives among the total number of actual positive cases. In this case, the average sensitivity is 90.41%.

SE = TP / (TP + FN) = 90.41%

c. Specificity (SP): Measures the proportion of true negatives among the total number of actual negative cases. In this case, the average specificity is 89.43%.

SP = TN / (TN + FP) = 89.43%

d. Precision (PREC): Measures the proportion of true positives among the total number of cases identified as positive. In this case, the average precision is 87.28%.

PREC = TP / (TP + FP) = 87.28%

These performance metrics indicate the overall effectiveness of the classification system in correctly identifying benign and malignant skin lesions. High values for accuracy, sensitivity, specificity, and precision suggest that the classifier is performing well in differentiating between benign and malignant cases.

4.4 RECEIVING RESULTS VIA WHATSAPP

The growing significance of telehealth in times of emergency brings to light the potential of mobile technology, like WhatsApp, as a means of text, audio, picture, and video messaging. This quick development in videoconferencing is especially helpful in far-off places or during pandemics when in-person talks might not be possible.

In such situations, the ability to send pathological diagnosis results to both the doctor and the patient can be extremely valuable. This approach enables healthcare providers to offer

continuous support and follow-up for patients dealing with acute and chronic dermatological conditions, especially during quarantine or periods of restricted movement.

By maintaining regular communication, patients can continue their therapy and receive guidance, minimizing the risk of treatment discontinuation and any negative clinical impact that may result from non-adherence. Although reducing face-to-face consultations is necessary to minimize the risk of disease exacerbation, telemedicine helps bridge the gap and ensure the continuity of care.

As previously stated, Figure 4.12 displays the program's communication to the physician in which the patient's melanoma is identified. This method of communication enables the patient to be continuously tracked regarding their state and reaction to therapy, ensuring they get the best care possible even in difficult situations.

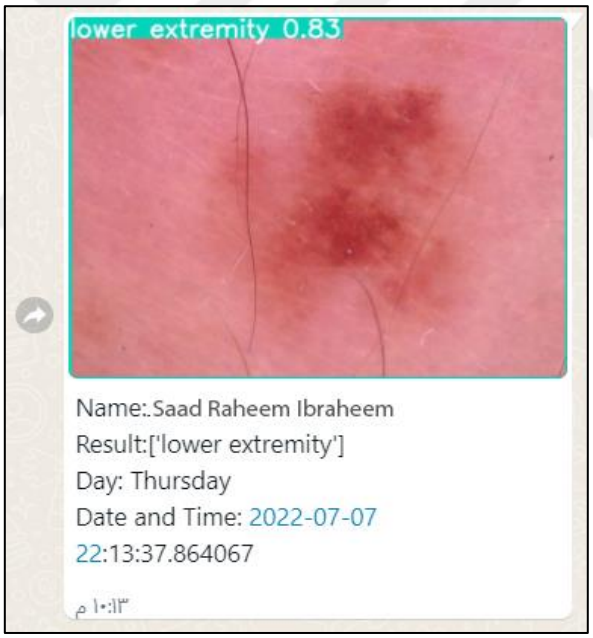

Figure 4.12: This Image Depicts A Sample of The Message That Our Program Transmits to The Doctor.

4.5 CHARACTERISTICS OF PATIENT

In this study, there 481 patients were examined, of whom 400 patients with 682 lesions were eligible for analysis. Propensity scores matching patient characteristics are detailed in (Figure 4.13).

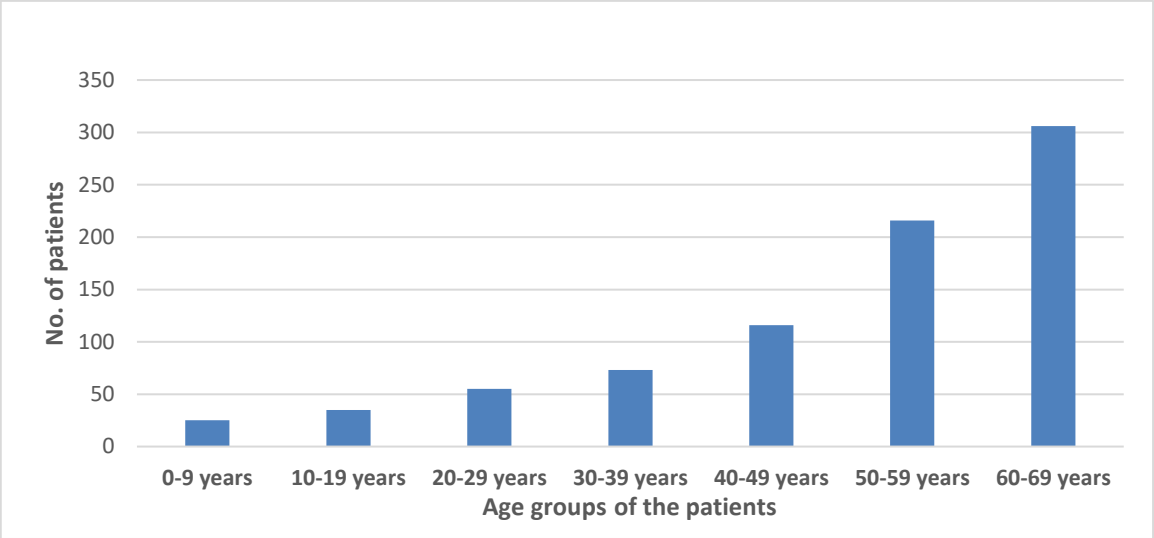

Figure 4.13: The Age Groups of The Patients

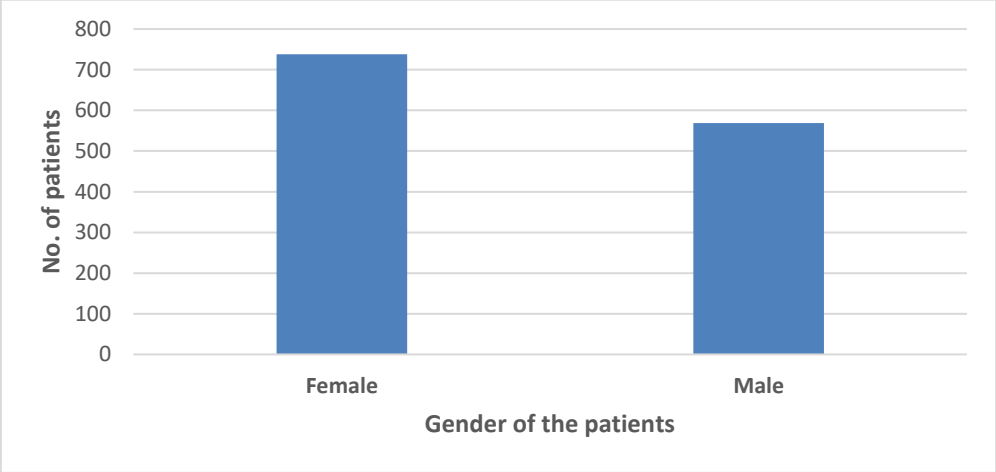

Figure 4.14: Shows the Number of Patients By Gender

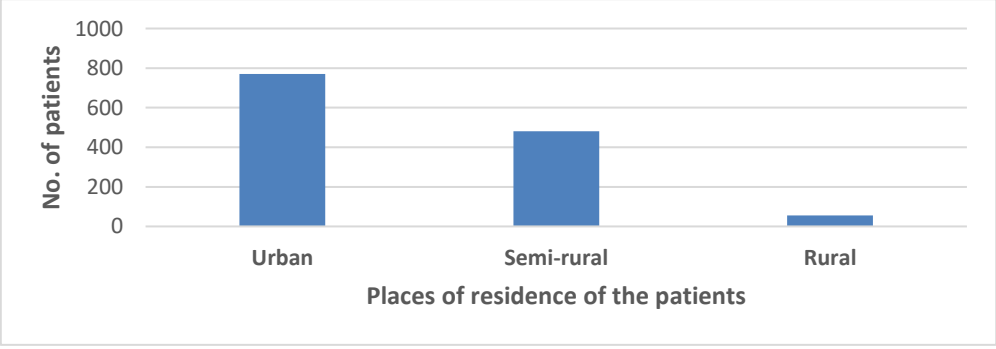

Figure 4.15: Shows The Number of Patients According to Their Places of Residence

4.5.1 Diagnostic Value of Patients Images

The average age of all patients in the study was 61 (p 0.001). (Figure 4.14). There were somewhat more women than men present (56%, 59%, and 64%). Although the percentage of rural patients was equal across groups, the percentage of semi-rural patients was significantly higher (60% for patients and 62% for referrers, p 0.01), as shown in (Figure 4.15).

Among the 45 patients that consulted a teledermatologist, 19 (or 4%) were never heard from again. Poor picture quality prevented the diagnosis of 71 lesions, or 5% of the total. The dermatologist was able to make a diagnosis for 115 of the lesions (9%) despite the low quality of the photos (Figure 4.16).

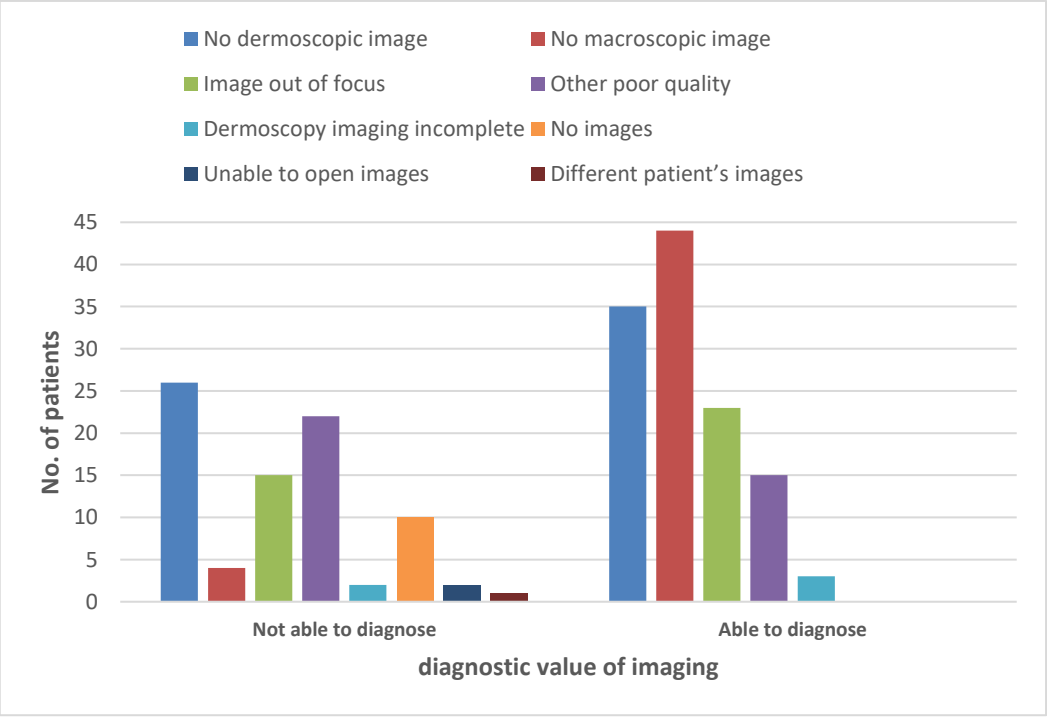

Figure 4.16: Shows The Diagnostic Value of Imaging For Lesions in The SSC Pathway

*Some lesions had more than one reason for inadequate quality.

4.5.2 Classification of Lesions

Malignant and non-malignant skin lesions were categorized according to their particular diagnoses. It was decided to create a subcategory for diagnoses with some uncertainty. Tele-dermatologists in the matched group had a 3.0 benign-to-malignant lesion ratio. Histopathological examination of malignant lesions showed a keratinocyte-to-melanocytic ratio of 1.8 in the matched cohort, (Figure 4.17). The ratio of minimally invasive to invasive melanomas was 3.70 in the matched cohort (Figure 4.18).

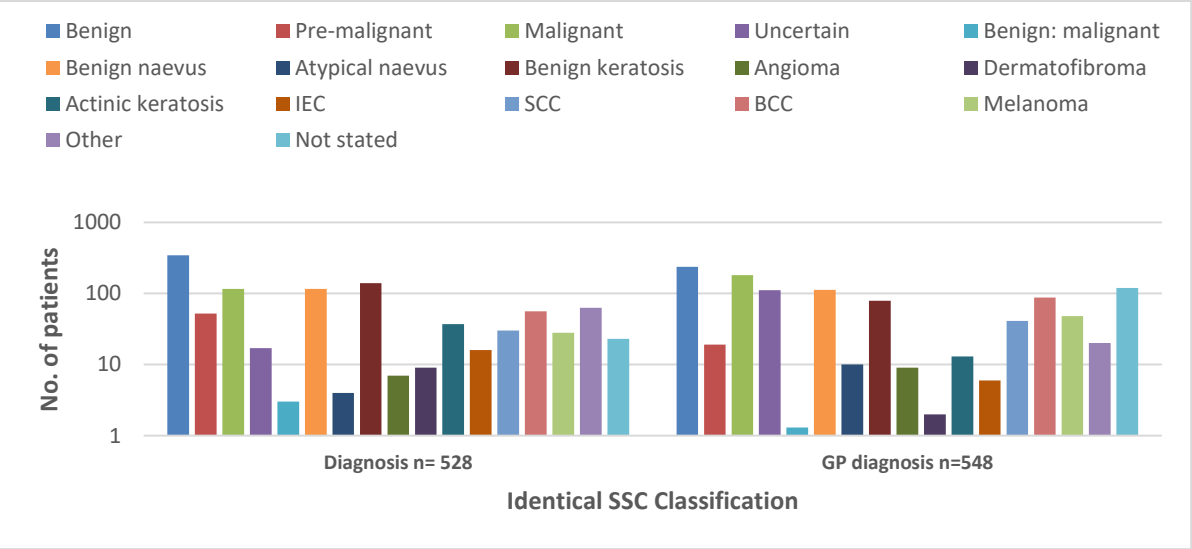

Figure 4.17: Shows the identical SSC Pathway Lesion Classification

*Compared to dermatologist diagnosis

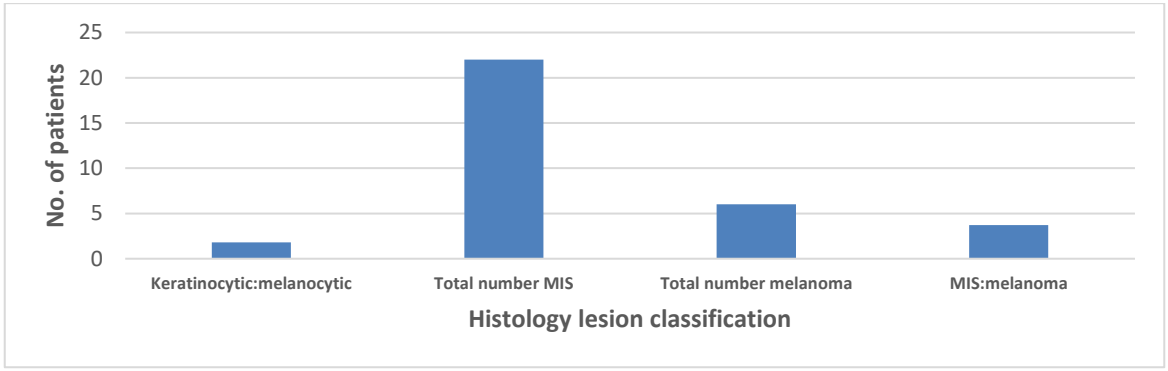

Figure 4.18: Shows the Histology Lesion Classification.

In 56, 57, and 69 percent of the SSC pairs, respectively, the dermatologist did not prescribe any further treatment. In the matched SSC, 26% of lesions were indicated for surgical therapy, including biopsy or excision (p 0.001).

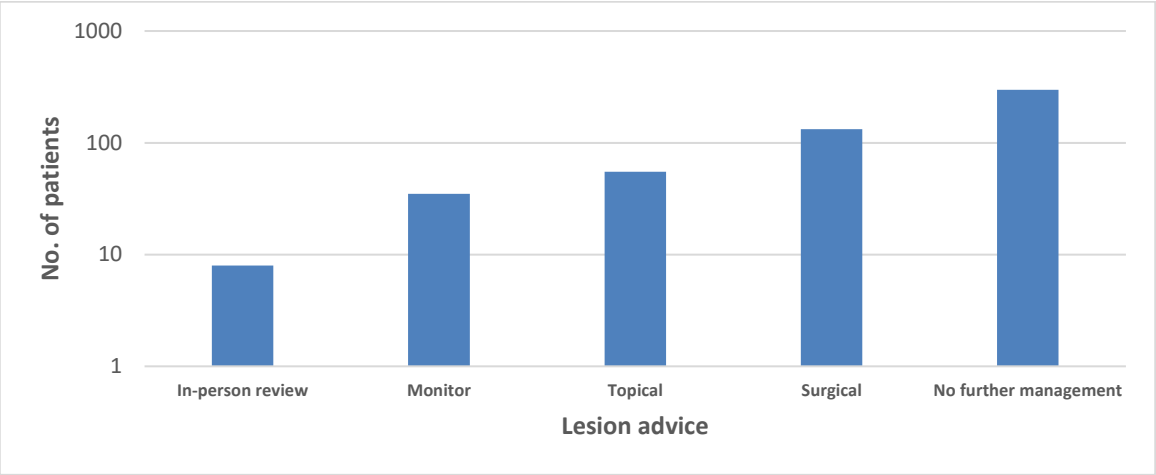

Figure 4.19: Shows The Lesion Advice on Patents

*Compared to matched SSC group

4.5.3 Similarity Between Diagnoses

For 528 lesions in the SSC pathway-matched cohort, diagnostic concordance between general practitioners and dermatologists was provided (Figure 4.19). There was statistically significant agreement between the SSC cohorts in determining whether or not a lesion was benign or malignant (58%; p 0.001). The particular diagnosis was agreed upon by 46% of patients in the SSC cohort.

a. The concordance of dermatologists and histopathologists in classifying lesions as benign or malignant was 70% for the SSC route group (p = 0.01). For a definitive diagnosis, the agreement between a dermatologist and histopathologists was 66% (53% complete, 13% partial), but it was only 48% (40% complete, 8% partial) between a general practitioner and histopathologists (p 0.001).

b. Consensus between dermatologists and pathologists for benign/malignant classification was 63%, but it was only 12% between general practitioners and

pathologists (p = 0.21). The rate of agreement between a dermatologist's diagnosis with the histology report was 65% (59% complete, 6% partial) but it was only 12% (6% complete, 6% partial) between general practitioners and histologists (p = 0.73).

c. When comparing dermatologists and pathologists, showed higher dermatologist-histology concordance (71% for benign/malignant categorization vs. GP-histology concordance, 49%, p = 0.001). The rate of agreement between a dermatologist's diagnosis and the histological findings was 57% (57% complete, 0% partial) (p = 0.03), but it was only 46% (41% complete, 5% partial) between a general practitioner's diagnosis with the histological findings.

There was no statistically significant difference (p=0.96) between the SSC in the rate of dermatologist-histology concordance in identifying benign/malignant skin lesions. In the SSC cohort, 34% of diagnoses were not in agreement. Eleven of the lesions (3%) were deemed benign by dermatologists but malignant by histology; four (3%) were found in the matched SSC route. Two of the lesions were recommended to be left alone, one lesion was recommended to be monitored, one lesion was recommended to get topical medication, one lesion was recommended to have excision/biopsy to clear up any uncertainty, and two lesions were recommended to be reviewed in person.

5. CONCLUSION AND FUTURE WORK

5.1 CONCLUSION

In this research, segmentation was done using thresholding and the k-means grouping method. The pre-processing stage employed a median filter for inpainting and the Sobel operator for border identification. In feature extraction methods, GLCM and LBP features were used to generate texture features, shape features, and intensity features. SVM was selected as the illness classification classifier.

The ISIC Archive supplied the information, and a 93% total success rate was attained. The results of the experiments show how well the suggested methods distinguish between innocuous and malignant tumors. This research tackles issues like the small intraclass variation of melanomas and the poor contrast of skin lesions.

Additionally, this research showed that telehealth could be used to evaluate and treat prevalent ambulatory dermatoses remotely. This approach reduces the risk of COVID-19 transmission and can be beneficial in remote or rural areas where access to healthcare facilities may be limited. The findings of this study highlight the potential of integrating machine learning and telemedicine to improve skin cancer detection and patient care in various settings.

5.2 FUTURE WORK

It is recommended that in subsequent work, the classifier's accuracy be increased by giving it more extracted characteristics and by analyzing bigger, more comprehensive datasets. This would make it possible for early-stage academics to use open-access datasets and standardized procedures in the battle against skin cancer.

Given the continuing COVID-19 pandemic, future research should also examine the expanded use of telemedicine for patient treatment and instructional reasons. As COVID-19 cases continue to rise globally, the findings of this study could contribute to enhancing telemedicine services, making them more effective and accessible to patients in need.

Additionally, researchers could investigate the integration of other machine learning techniques or deep learning models to further enhance the performance and generalization capabilities of the system. Exploring the use of real-time video consultations, along with the incorporation of dermoscopic images, could also help improve diagnostic accuracy and patient engagement.

By building upon the findings of this study, the medical community can continue to advance the field of telemedicine and remote diagnostics, ultimately improving patient care and accessibility to healthcare services in various settings.

REFERENCES

[1] U. Atique, S. Mushtaq, I. A. Rana, and U. Hassan, "Clinicopathologic Features of Cutaneous Malignant Melanoma and Their Impact on Prognosis," *Cureus*, vol. 12, no. 9, 2020.

[2] L. Jones, "Remote skin cancer diagnosis: A comparison of the Waikato District Health Board's Suspected Skin Cancer pathway in 2020 with the Virtual Lesion Clinic in 2020 and 2016".

[3] P. Pyramid, "Population Pyramids of the World from 1950 to 2100-Sri Lanka. 2019 [cited 2020-06-05]." 2019.

[4] P. R. Cyr, W. Craig, H. Ahrns, K. Stevens, C. Wight, and E. Seiverling, "Teaching Skin Cancer Detection to Medical Students Using a Dermoscopic Algorithm," *PRiMER: Peer-Review Reports in Medical Education Research*, vol. 5, 2021.

[5] J. Rockberg, J. M. Amelio, A. Taylor, L. Jörgensen, P. Ragnhammar, and J. Hansson, "Epidemiology of cutaneous melanoma in Sweden—stage-specific survival and rate of recurrence," *Int J Cancer*, vol. 139, no. 12, pp. 2722–2729, 2016.

[6] C. Skayem *et al.*, "Teledermatology for COVID-19 cutaneous lesions: substitute or supplement?," *Journal of the European Academy of Dermatology and Venereology*, 2020.

[7] P. Pasquali *et al.*, "Teledermatology and its current perspective," *Indian Dermatol Online J*, vol. 11, no. 1, p. 12, 2020.

[8] N. C. F. Codella *et al.*, "Skin lesion analysis toward melanoma detection: A challenge at the 2017 international symposium on biomedical imaging (isbi), hosted by the international skin imaging collaboration (isic)," in *2018 IEEE 15th international symposium on biomedical imaging (ISBI 2018)*, 2018, pp. 168–172.

[9] Z. Zhao, Z. Liu, and M. Larson, "Towards large yet imperceptible adversarial image perturbations with perceptual color distance," in *Proceedings of the IEEE/CVF Conference on Computer Vision and Pattern Recognition*, 2020, pp. 1039–1048.

[10] K. Yunus and T. Ölmez, “Improved fuzzy c-means and k-means algorithms for texture and boundary segmentation,” in *2018 6th International Conference on Control Engineering & Information Technology (CEIT)*, 2018, pp. 1–6.

[11] M. Nasir, M. Attique Khan, M. Sharif, I. U. Lali, T. Saba, and T. Iqbal, “An improved strategy for skin lesion detection and classification using uniform segmentation and feature selection based approach,” *Microsc Res Tech*, vol. 81, no. 6, pp. 528–543, 2018.

[12] T. Mendonça, P. M. Ferreira, J. S. Marques, A. R. S. Marcal, and J. Rozeira, “PH 2-A dermoscopic image database for research and benchmarking,” in *2013 35th annual international conference of the IEEE engineering in medicine and biology society (EMBC)*, 2013, pp. 5437–5440.

[13] A. T. Simin, S. M. G. Baygi, and A. Noori, “Cancer Diagnosis Based on Combination of Artificial Neural Networks and Reinforcement Learning,” in *2020 6th Iranian Conference on Signal Processing and Intelligent Systems (ICSPIS)*, 2020, pp. 1–4.

[14] S. S. Mohammed and J. M. Al-Tuwaijari, “Skin Disease Classification System Based on Machine Learning Technique: A Survey,” in *IOP Conference Series: Materials Science and Engineering*, 2021, vol. 1076, no. 1, p. 12045.

[15] S. Sreena and A. Lijiya, “Skin lesion analysis towards melanoma detection,” in *2019 2nd International Conference on Intelligent Computing, Instrumentation and Control Technologies (ICICICT)*, 2019, vol. 1, pp. 32–36.

[16] M. A. Farooq, M. A. M. Azhar, and R. H. Raza, “Automatic lesion detection system (ALDS) for skin cancer classification using SVM and neural classifiers,” in *2016 IEEE 16th International Conference on Bioinformatics and Bioengineering (BIBE)*, 2016, pp. 301–308.

[17] E. M. Senan and M. E. Jadhav, “Techniques for the Detection of Skin Lesions in PH 2 Dermoscopy Images Using Local Binary Pattern (LBP),” in *International Conference on Recent Trends in Image Processing and Pattern Recognition*, 2020, pp. 14–25.

[18] M. Prathiba, D. Jose, R. Saranya, and others, “Automated melanoma recognition in dermoscopy images via very deep residual networks,” in *IOP Conference Series: Materials Science and Engineering*, 2019, vol. 561, no. 1, p. 12107.

[19] H. Nahata and S. P. Singh, “Deep learning solutions for skin cancer detection and diagnosis,” *Machine Learning with Health Care Perspective: Machine Learning and Healthcare*, pp. 159–182, 2020.

[20] H. Lee and Y.-P. P. Chen, “Image based computer aided diagnosis system for cancer detection,” *Expert Syst Appl*, vol. 42, no. 12, pp. 5356–5365, 2015.

[21] M. A. Albahar, “Skin lesion classification using convolutional neural network with novel regularizer,” *IEEE Access*, vol. 7, pp. 38306–38313, 2019.

[22] T. Saba, “Computer vision for microscopic skin cancer diagnosis using handcrafted and non-handcrafted features,” *Microsc Res Tech*, vol. 84, no. 6, pp. 1272–1283, 2021.

[23] P. Banasode, M. Patil, and N. Ammanagi, “A melanoma skin cancer detection using machine learning technique: support vector machine,” in *IOP Conference Series: Materials Science and Engineering*, 2021, vol. 1065, no. 1, p. 12039.

[24] F. Renard, S. Guedria, N. de Palma, and N. Vuillerme, “Variability and reproducibility in deep learning for medical image segmentation,” *Sci Rep*, vol. 10, no. 1, pp. 1–16, 2020.

[25] N. Razmjooy and S. Razmjooy, “Skin melanoma segmentation using neural networks optimized by quantum invasive weed optimization algorithm,” in *Metaheuristics and optimization in computer and electrical engineering*, Springer, 2020, pp. 233–250.

[26] P. Singh, M. Kumar, and A. Bhatia, “A Comparative Analysis of Deep Learning Algorithms for Skin Cancer Detection,” in *2022 6th International Conference on Intelligent Computing and Control Systems (ICICCS)*, 2022, pp. 1160–1166.

[27] N. Zhang, Y.-X. Cai, Y.-Y. Wang, Y.-T. Tian, X.-L. Wang, and B. Badami, “Skin cancer diagnosis based on optimized convolutional neural network,” *Artif Intell Med*, vol. 102, p. 101756, 2020.

[28] H.-Y. Huang, Y.-P. Hsiao, A. Mukundan, Y.-M. Tsao, W.-Y. Chang, and H.-C. Wang, "Classification of Skin Cancer Using Novel Hyperspectral Imaging Engineering via YOLOv5," *J Clin Med*, vol. 12, no. 3, p. 1134, 2023.

[29] P. Tschandl, "The HAM10000 dataset, a large collection of multi-source dermatoscopic images of common pigmented skin lesions." Harvard Dataverse, 2018. doi: 10.7910/DVN/DBW86T.

[30] Y. Li and L. Shen, "Skin lesion analysis towards melanoma detection using deep learning network," *Sensors*, vol. 18, no. 2, p. 556, 2018.

[31] M. S. K. C. Center, "The International Skin Imaging Collaboration (ISIC) ." 2019. [Online]. Available: https://www.isic-archive.com/#!/topWithHeader/wideContentTop/main

[32] J. Chen, T. Luo, J. Wu, Z. Wang, and H. Zhang, "A Vision Transformer network SeedViT for classification of maize seeds," *J Food Process Eng*, vol. 45, no. 5, p. e13998, 2022.

[33] R. Jose, "A convolutional neural network (cnn) approach to detect face using tensorflow and keras," *International Journal of Emerging Technologies and Innovative Research, ISSN*, pp. 2349–5162, 2019.

[34] Alejandro Escontrela, "Understanding Convolutional Neural Network." May 2021. [Online]. Available: https://medium.com/@zaralwinneirin/understanding-convolutional-neural-network-20893de2a105

[35] L. Alzubaidi *et al.*, "Review of deep learning: Concepts, CNN architectures, challenges, applications, future directions," *J Big Data*, vol. 8, pp. 1–74, 2021.

[36] U.-O. Dorj, K.-K. Lee, J.-Y. Choi, and M. Lee, "The skin cancer classification using deep convolutional neural network," *Multimed Tools Appl*, vol. 77, pp. 9909–9924, 2018.

[37] M. A. Ottom, "Convolutional Neural Network for diagnosing skin cancer," *Int. J. Adv. Comput. Sci. Appl*, vol. 10, no. 7, pp. 333–338, 2019.

[38] K. Ali, Z. A. Shaikh, A. A. Khan, and A. A. Laghari, "Multiclass skin cancer classification using EfficientNets–a first step towards preventing skin cancer," *Neuroscience Informatics*, vol. 2, no. 4, p. 100034, 2022.

[39] J. Wu, "Introduction to convolutional neural networks," *National Key Lab for Novel Software Technology. Nanjing University. China*, vol. 5, no. 23, p. 495, 2017.

[40] S. Gutta, "Object detection algorithm-yolo v5 architecture." Aug, 2021.

[41] R. Refianti, A. B. Mutiara, and R. P. Priyandini, "Classification of melanoma skin cancer using convolutional neural network," *International Journal of Advanced Computer Science and Applications*, vol. 10, no. 3, 2019.

[42] M. A. Linares, A. Zakaria, and P. Nizran, "Skin cancer," *Primary care: Clinics in office practice*, vol. 42, no. 4, pp. 645–659, 2015.

[43] W. Python, "Python," *Python Releases for Windows*, vol. 24, 2021.

[44] J. Jaworek-Korjakowska, "Computer-aided diagnosis of micro-malignant melanoma lesions applying support vector machines," *Biomed Res Int*, vol. 2016, 2016.

[45] J. Jaworek-Korjakowska and P. Kłeczek, "Automatic classification of specific melanocytic lesions using artificial intelligence," *Biomed Res Int*, vol. 2016, 2016.

[46] M. Y. Su and S. Das, "Expansion of asynchronous teledermatology during the COVID-19 pandemic," *J Am Acad Dermatol*, vol. 83, no. 6, pp. e471–e472, 2020.

[47] S. Bergamo *et al.*, "Teledermatology with general practitioners and pediatricians during COVID-19 outbreak in Italy: Preliminary data from a second-level dermatology department in North-Eastern Italy," *Dermatol Ther*, vol. 33, no. 6, 2020.

[48] R. Kazi *et al.*, "Utilization of asynchronous and synchronous teledermatology in a large health care system during the COVID-19 pandemic," *Telemedicine and e-Health*, vol. 27, no. 7, pp. 771–777, 2021.

[49] M. Farshchian, G. Potts, A. Kimyai-Asadi, D. Mehregan, and S. Daveluy, "Outpatient Teledermatology Implementation During the COVID-19 Pandemic: Challenges and Lessons Learned.," *J Drugs Dermatol*, vol. 19, no. 6, p. 683, 2020.

[50] C. Marasca, A. Ruggiero, G. Fontanella, M. Ferrillo, G. Fabbrocini, and A. Villani, "Telemedicine and support groups in order to improve the adherence to treatment and health related quality of life in patients affected by inflammatory skin conditions during COVID-19 emergency," *Clin Exp Dermatol*, p. e14245, 2020.

[51] A. Morrone, A. Cristaudo, M. Ardigò, P. Frascione, A. Pacifico, and M. Giuliani, "Rescheduling of clinical activities and teleconsulting for public dermatology. Two prompt answers to COVID-19 emergency," *Int J Dermatol*, 2020.

[52] M. R. McCrary, T. Rogers, H. Yeung, L. Krueger, and S. C. Chen, "Abstract PO-042: Would dermoscopic photographs help triage teledermatology consults in the COVID-19 era?," *Clinical Cancer Research*, vol. 26, no. 18_Supplement, p. PO–042, 2020.

[53] M. Randolph, A. Al-Alola, and A. Tosti, "Diagnosis of hair disorders during the COVID-19 pandemic: an introduction to teletrichoscopy," *Journal of the European Academy of Dermatology and Venereology*, vol. 35, no. 3, p. e167, 2021.

[54] C. R. McDonald, L. Watson, T. Shim, and A. Ilchyshyn, "Community-based medical photography improves skin cancer teledermatology triage during the national COVID-19 pandemic," *British Journal of Dermatology*, p. 207, 2020.

[55] A. M. Cartron, K. Rismiller, and J. C. L. Trinidad, "Store-and-forward teledermatology in the era of COVID-19: A pilot study.," *Dermatol Ther*, vol. 33, no. 4, pp. e13689–e13689, 2020.

[56] A. A. Marghoob, "International Skin Imaging Collaboration Melanoma Project Working G," *Standards in Dermatologic Imaging. JAMA Dermatol.*, vol. 151, no. 8, pp. 819–821, 2015.

[57] R. Javed, M. S. M. Rahim, T. Saba, and A. Rehman, "A comparative study of features selection for skin lesion detection from dermoscopic images," *Network Modeling Analysis in Health Informatics and Bioinformatics*, vol. 9, no. 1, pp. 1–13, 2020.